AAC Accepted Manuscript Posted Online 11 February 2019
Antimicrob. Agents Chemother. doi:10.1128/AAC.02061-18

Optimization of methionyl tRNA-synthetase inhibitors for treatment of *Cryptosporidium* infection

Frederick S. Buckner[a*], Ranae M. Ranade[a], J. Robert Gillespie[a], Sayaka Shibata[b], Matthew A. Hulverson[a], Zhongsheng Zhang[b], Wenlin Huang[b], Ryan Choi[a], Christophe L. M. J. Verlinde[b], Wim G. J. Hol[b], Atsuko Ochida[c], Yuichiro Akao[c], Robert K.M. Choy[d] Wesley C. Van Voorhis[a], Sam L.M. Arnold[a], Rajiv S. Jumani[e], Christopher D. Huston[e], Erkang Fan[b*]

Affiliations: Department of Medicine[a] and Department of Biochemistry[b], University of Washington, Seattle, Washington, USA; Takeda Pharmaceuticals[c], Osaka, Japan; Drug Development Program[d], PATH, San Francisco, CA, USA; Department of Medicine[e], University of Vermont, Burlington, Vermont, USA.

* Corresponding authors:

Frederick S. Buckner: fbuckner@uw.edu

Erkang Fan: erkang@uw.edu

ABSTRACT: Cryptosporidiosis is one of the leading causes of moderate to severe diarrhea in children in low-resource settings. The therapeutic options for cryptosporidiosis are limited to one drug, nitazoxanide, which unfortunately has poor activity in the most needy populations of malnourished children and HIV infected persons. This paper describes the discovery and early optimization of a class of imidazopyridine-containing compounds with potential for treating *Cryptosporidium* infections. The compounds target the *Cryptosporidium* methionyl-tRNA synthetase (MetRS), an enzyme that is essential for protein synthesis. The most potent compounds inhibited the enzyme with K_i values in the low picomolar range. *Cryptosporidium* cells in culture were potently inhibited with EC_{50} values as low 7 nM and >1000-fold selectivity over mammalian cells. A parasite persistence assay indicates that the compounds act by a parasiticidal mechanism. Several compounds were demonstrated to control infection in two murine models of cryptosporidiosis without evidence of toxicity. Pharmacological and physicochemical characteristics of compounds were investigated to determine properties that were associated with higher efficacy. The results indicate that MetRS inhibitors are excellent candidates for development for anti-cryptosporidiosis therapy.

INTRODUCTION:

Although the world has seen substantial progress in the reduction of child mortality in recent decades, much work remains to achieve the United Nations' Sustainable Development Goals (targeting 2030) for child survival (1). Diarrhea is one of the leading causes of child mortality, responsible for 8% of deaths in children aged 1-59 months (2). The Global Enteric Multicenter Study (GEMS) identified *Cryptosporidium* to be the second leading cause of moderate to severe diarrhea in young children at sites in Africa and Asia (3). The importance of cryptosporidiosis in community diarrhea in developing countries was confirmed in the MAL-ED study (4). Beyond the mortality risk, children who survive cryptosporidiosis suffer from growth and developmental stunting which contribute to all-cause mortality and disability (5, 6). The recent appreciation of the impact of cryptosporidiosis has drawn attention to the inadequacies in the means to control this infectious disease. No vaccines are in clinical use and the sole drug for treating cryptosporidiosis (nitazoxanide) has poor efficacy in malnourished children and in patients with human immunodeficiency virus. Vaccine development is likely to be slow due to difficulties raised by antigenic differences within *Cryptosporidium* leading to poor cross protection between species and strains (7). New anticryptosporidial drugs are likely to be the most rapidly developed technology to address the burden of *Cryptosporidium* infection.

Recent studies suggest that *Cryptosporidium* is more closely related to gregarine protozoa than to coccidians (8). The genus *Cryptosporidium* has 27 species that have been identified worldwide that infect four classes of vertebrates (9). The species

primarily responsible for human cryptosporidiosis are *C. hominis* and *C. parvum*. Water- and foodborne transmission are the major modes of infection, although person to person contact is also described (9). The small intestine is the primary site of *Cryptosporidium* infection in humans, although extra-intestinal sites such as the biliary tract, lungs, and pancreas can be involved in immune compromised and immune competent individuals (9-11). The extra-intestinal locations may have important implications for developing therapeutics that act at all sites of infection. *Cryptosporidium* mainly resides in an unusual niche in the intestinal epithelium known as the parasitophorous vacuole, which is insulated from both the intestinal lumen as well as the host cytoplasm. Therefore, it is not entirely known whether anti-*Cryptosporidium* drugs should be optimized for luminal or plasma exposure, although a recent paper emphasizes the importance of gastrointestinal (luminal) exposure in a murine model (12).

Protein synthesis is a classic antimicrobial drug target, dating back to many of the first antibiotics—such as chloramphenicol, tetracycline and erythromycin—that inhibit bacterial protein synthesis. Recently, aminoacyl-tRNA synthetase (aaRS) inhibitors have emerged as promising therapeutic candidates for targeting protein synthesis. Using ATP hydrolysis, aaRSs catalyze the formation of tRNAs charged with their cognate amino acids which serve as the substrates for the formation of new peptides. Mupirocin, a small molecule inhibitor of isoleucyl-tRNA synthetase (13), has been in clinical use for more than two decades as a topical treatment for *Staphylococcus* infections. Tavaborole is a leucyl-tRNA synthetase inhibitor that was approved by the FDA in 2014 for topical treatment of onychomycosis (14, 15). Halofuginone, a prolyl-tRNA synthetase inhibitor (16), is approved for veterinary use against *Cryptosporidium* in Europe, although a narrow therapeutic index makes it unsuitable for human use. Three different aaRS inhibitors for systemic use are in clinical trials, demonstrating the potential for safe use beyond topical applications. These include the methionyl-tRNA synthetase (MetRS) inhibitor CRS3213 for *Clostridium difficile* infections (ClinicalTrials.gov, NCT01551004), the leucyl-tRNA synthetase inhibitor GSK2251052 for Gram-negative bacterial infections (17, 18), and the leucyl-tRNA synthetase inhibitor GSK3936656 for multidrug resistant tuberculosis (19, 20). Inhibitors of other aaRSs from protozoan parasites including *Cryptosporidium, Plasmodium*, *Trypanosoma* and *Toxoplasma* are also in development (21, 22).

MetRS enzymes fall into two categories, MetRS1 and MetRS2 (23). *C. parvum* and *C. hominis* contain a single MetRS gene that aligns with the MetRS1 category, meaning it has close homology to the MetRS of *S. aureus, Trypanosoma spp.,* and the human mitochondrial MetRS. Our group has been developing inhibitors to type 1 MetRS that are shown to have potent activity against trypanosomes and Gram positive bacteria, including activity in animal models (24-27). Supporting this work are numerous crystal structures of the inhibitors bound to the *Trypanosoma brucei* MetRS

enzyme (28-30), which is 76% identical (19 of 25 residues) to the *C. parvum/hominis* MetRS within the inhibitor binding pocket. In this paper, the *C. parvum* MetRS was characterized and MetRS inhibitors were shown to be highly potent with K_i values as low as 0.9 pM. Compound **2093** had the most potent in vitro activity against *C. parvum*, and reduced *Cryptosporidium* infection to low levels in two murine models without showing signs of toxicity. The physicochemical and pharmacological features associated with in vivo activity are discussed. The research illustrates the potential of target-based drug discovery to develop a novel therapeutic against a formidable eukaryotic pathogen.

RESULTS

Amino acid sequence alignment. *Cryptosporidium parvum* (UniProt Q5CVN0) and *Cryptosporidium hominis* (UPI0000452AB0) have a single MetRS gene in their respective genomes. These sequences were compared to the well-characterized *Trypanosoma brucei* MetRS by mapping them onto the crystal structures of *Tb*MetRS bound to inhibitors. Table 1 shows the amino acid residues of *Tb*MetRS that form binding pockets that are in direct proximity to MetRS inhibitors (28-30). The *C. parvum* and *C. hominis* sequences are identical to each other over the 25 residues forming the compound binding pockets. The *Cryptosporidium* sequences share 19 identical amino acids with *Tb*MetRS and 18 identical residues with the human mitochondrial MetRS over this region. Only 14 of the 25 amino acids are identical between the *Cryptosporidium* MetRS and the human cytoplasmic MetRS in this region.

Enzymology. The *C. parvum* MetRS enzyme was over-expressed in *E. coli* and purified by nickel affinity chromatography followed by size exclusion chromatography (Fig. S1, Supplementary Data). The activity was confirmed in the aminoacylation assay which detects the esterification of radiolabeled methionine to the tRNA substrate (Fig. S2, Supplementary Data). However, in order to measure the Michaelis-Menten constants for the enzyme, the ATP:PP_i exchange assay was employed as previously explained (31). The K_m for the methionine substrate was comparable to that observed in *S. aureus* (both in house and published) (Table 2), but about 4-fold higher than the value for the human mitochondrial MetRS (71 vs. 18 µM). The K_m for the ATP substrate was about 2-3 fold higher than that observed in *S. aureus* (both in house and published) (Table 2), and about 10-fold higher than the value for the human mitochondrial MetRS (1040 vs. 85 µM).

MetRS inhibitor activities. The initial MetRS inhibitors were synthesized to target trypanosomatid parasites (24-26, 30). The activities of selected compounds on: *Cp*MetRS enzyme, *C. parvum* parasites cultured in HCT-8 cells, and mammalian cells are shown in Tables 3 and 4. The MetRS inhibitors are characterized by two ring

systems tethered by a linker. Table 3 shows four compounds in which the linker is an alkyl chain ("linear linker"). The aminoquinolone (**1312**) (24) and urea-containing compounds (**1433**) (25) are weakly active on the *Cp*MetRS enzyme and show little activity on *C. parvum* cultures. The fluoro-imidazopyridine compounds (**1614** and **1717**) (26) have moderate activity on both the enzyme and cultures. Next, a series of 13 compounds containing a ring in the linker region were tested (Table 4). The 1,3-dihydro-2-oxo-imidazole ring was found to be the most active and thus variants of this scaffold were further investigated. Compound **2093** is the overall most potent compound with a K_i value on *Cp*MetRS of 0.9 pM and an EC_{50} between 7 nM and 36 nM determined in independent laboratories using different readout techniques (luciferase reporter vs. fluorescence microscopy) and different *C. parvum* strains (see Methods). Importantly, **2093** has no cytotoxicity on mammalian cells at the highest (50 µM) concentration tested. Examining the SAR of this scaffold indicates the relative potency at the R_1 position as follows: ethyl>CH_2CF_2H> propyl>H. At the R_2 position, Cl is slightly better than F (compare **2093** to **2114** and **2067** to **2062**). Finally, at R_3 the methoxy substitution provides moderately greater potency than chloro (compare **2114** to **2062** or **2093** to **2067** or **2258** to **2138**). None of the compounds exhibited substantial cytotoxicity on either mammalian cell line tested (CRL-8155 or HepG2).

The correlation between enzyme inhibitory activity and *C. parvum* growth inhibitory activity was plotted for all the compounds shown in Tables 3 and 4. A strong correlation was observed (R^2 = 0.91) (Figure 1).

The compounds were also tested for inhibitory activity of mitochondrial protein synthesis in HepG2 cells (COX-1 EC_{50}, Tables 3 and 4). The COX-1 gene is encoded by the mitochondrial genome and expressed in the mitochondrial protein synthesis pathway. The MetRS inhibitors showed a wide range of EC_{50} values from low micromolar to low nanomolar concentrations. In general, compounds with potent activity on *C. parvum* cultures also had potent activity on the COX-1 enzyme (e.g., **2093**). A parallel experiment was performed on the same samples to measure levels of the nuclear encoded SDH-A protein that is imported into the mitochondrion. A reduction in levels of this protein reflects general toxicity to the cells. Except for compound **1433**, all compounds exhibited SDH-A EC_{50} values >25 µM, indicating no general toxicity at this concentration.

The activity of the most potent MetRS inhibitor, **2093**, was tested against a panel of three different *C. parvum* strains including a clinical isolate from dairy calves and a *C. hominis* strain (Table S1, Supplementary data). Compound **2093** had EC_{50} values ranging from 0.006 – 0.029 µM against *C. parvum* strains and of 0.015 µM against *C. hominis.* A wide therapeutic index was also documented with CC_{50} values >25 µM against 3 mammalian cell lines.

Next, a parasite persistence assay was performed with **2093** and control compounds nitazoxanide and MMV665917 (Fig. 2). The persistence curve for **2093**

closely resembles that of MMV665917 which is believed to have a parasiticidal mechanism of anti-*Cryptosporidium* activity and is dissimilar to the curve for nitazoxanide which is believed to have a parasitistatic mechanism (32).

Efficacy in two murine *C. parvum* infection models.

Compounds with the highest in vitro potency were selected for efficacy studies employing two different mouse models.

NOD SCID Gamma (NSG) mouse model (32): Adult mice (n=4 per group) received a challenge dose of 10^5 oocysts and were treated with study compounds from day 6-10 post-infection. Parasites were quantified in stool by PCR on day 5 and day 11 post-infection showing that **2093** was associated with 98.6% reduction ($P<0.05$) of parasites. Compound **2069** resulted in 83.6% reduction (($P<0.05$), whereas compound **2067** had only an 8.9% reduction (not statistically significant) (Fig. S3, Expt 1). A follow up experiment showed similar results for **2093** and about the same level of parasite reduction with **2259** (Fig. S3, Expt 2, $P<0.05$ for both compounds).

IFN-γ knockout mouse model (33): Efficacy experiments were also performed using adult IFN-γ knockout mice and a luciferase expressing *C. parvum* strain. Adult mice (n=3 per group) received a challenge dose of 10^3 oocysts, and like above, were treated with study compounds from day 6-10 post-infection. Pooled feces from each group were collected daily and the parasite load was quantified by luminometry. Again, **2093** was found to be highly efficacious (>4 $\log_{10}$ drop in luminescence) at the oral dose of 50 mg/kg BID (Fig 3A). Compound **2093** was also tested at lower doses of 50 mg/kg once per day (Fig. 3B) and at 25 mg/kg twice per day (Fig. 3C), and resulted in ~3-$\log_{10}$ drop in fecal parasite levels in both experiments. At 20 mg/kg once per day, **2093** gave ~1-$\log_{10}$ drop in parasite levels (day 9) that then rebounded to control levels after the treatment was completed (Fig. 3D). Compound **2114** and **2259** at 50 mg/kg BID gave similar profiles to **2093** with a 3-4 $\log_{10}$ drop in stool parasite levels (Fig. 3E and 3F), whereas compounds **2258** appeared less active (Fig. 3C). Other compounds with modest anticryptosporidial activity (1-2 log drop in fecal parasite loads) were **2138** and **2139** (Figs. 3G). Finally, the following compounds had no demonstrable activity: **2207** at 50 mg/kg PO QD nor **2080**, **2240** or **2242** given at 25 mg/kg PO BID (data not shown). A control compound with strong anti-*Cryptosporidium* activity, the "bumped kinase inhibitor" **1369** (33), was included in some experiments for reference (Figures 3F and 3G).

In all experiments, the mice were weighed daily. Weight loss was consistently observed in the mice treated with vehicle control. When weights drop below 20% of baseline, mice were euthanized per protocol requirements. (The lines end when all mice were culled). There was some variability between experiments in the time it took for control mice to reach terminal weight (e.g., compare panel 3A to panel 3F). The mice receiving treatments that led to reduced *Cryptosporidium* infection had relatively

stable weights over the course of the experiment. Once the compound dosing was completed (day 11), weight gain was sometimes observed (e.g. panel 3A and 3G). Except for compound **2258**, the MetRS inhibitors shown in Fig. 3 were well-tolerated and led to all mice surviving (without >20% weight loss) until the end of the experiment.

Physicochemical properties, metabolism, pharmacokinetic studies.

Physicochemical properties of the compounds were calculated or measured (Table 5). The molecular weights for the ring-linker series are in the 400 – 500 g/mol range. The calculated log P values range from 3.25 to 4.75. Solubility of **2093, 2114,** and **2259** (the more active compounds in the mouse efficacy model) was higher than for **2067** and **2069**. Plasma protein binding is high for all of the tested compounds, ranging from 95% to >99.9%, with the exception of **2240** with a plasma protein binding value of 87.7%. Permeability was assessed for a subset of compounds using the PAMPA method and showed fairly similar permeability values (226-319 nm/sec) for the tested compounds. For comparison, a highly permeable compound, propranolol, had a permeability value of 600 nm/sec (pH 7.4) and a low permeability compound, methylclothiazide, has a value of 30 nm/sec (pH 7.4). The permeability of the compounds was also calculated by computer algorithm, and indicated that the predicted permeability for MetRS inhibitors is more similar to propranolol (known to have high permeability) than methylclothiazide (known to have low permeability). The relationship between the described chemical properties (i.e., the predicted permeability and the solubility/EC_{50}) and in vivo efficacy of the compounds was graphed (Fig. 4). This shows that the most active compounds in vivo cluster at an intermediate level of permeability and have a high ratio of solubility/EC_{50}.

In vitro measurements of liver microsome stability showed half-lives ranging from 2-29 min (mouse) and 8-42 min (human) (Table 6). The blood pharmacokinetics in mice were measured following a single oral dose of 50 mg/kg. Peak blood levels (C_{max}) and area under the curve (AUC) are shown in Table 6. Compound **2067** had the highest C_{max} (65 µM) and AUC (17263 min*µM/L), whereas compound **2093** had a lower exposure in blood: C_{max} (5.8 µM) and AUC (1863 min*µM/L). Levels of compounds were also measured in the feces of selected compounds and were observed to be in the 10-50 µM range with the exception of **2240** for which fecal levels were very high at 846 µM.

Safety studies. The compounds with the best in vivo activity (**2093**, **2114**, and **2259**) were tested for inhibition of five human CYP isoenzymes at a single 10 µM concentration. Similar results were observed for all three compounds. Only CYP2C8 was inhibited by >50% at this concentration (Table 7). Inhibition of the hERG channels was measured at two concentrations, 10 and 30 µM (Table 8). Again, similar results were observed for three compounds. In the absence of serum, hERG inhibition was

approximately 60% at 30 µM, but the inhibition dropped to ~20% in the presence of BSA. The Ames and in vitro micronucleus tests for genotoxicity were done on **2093** and both found to be negative. Detailed results are available in the supplementary data section.

DISCUSSION

The *Cryptosporidium* enzyme, methionyl-tRNA synthetase, was targeted for the development of novel drugs to treat cryptosporidiosis. Analysis of the deposited amino acid sequence of the *Cp*MetRS revealed that it clusters with type 1 MetRS enzymes (23) that include trypanosomes, *Giardia*, and Gram positive bacteria. In previous work, crystal structures of the *T. brucei* MetRS revealed the ATP and methionine binding pockets as well as the binding mode for numerous inhibitors (28, 29). By mapping the *C. parvum* enzyme to the *T. brucei* MetRS structure, the analogous binding pocket was identified, demonstrating that 19 of 25 amino acids (76%) forming the surface of the pocket are identical. This indicated that inhibitors of the *T. brucei* MetRS would be likely to bind the *Cp*MetRS. The binding pocket residues of the *C. hominis* MetRS are identical to those of *C. parvum.* The sequence analysis also showed that 18 of 24 residues (75%) were identical in the corresponding human mitochondrial MetRS. The significance of this similarity is discussed below. In contrast, the human cytoplasmic MetRS had a lower degree of identity, 14 of 24 (58%) which is consistent with the knowledge that the human cytoplasmic MetRS belongs to the MetRS2 category which is not inhibited by the compounds under investigation.

The *Cp*MetRS gene was amplified from genomic DNA, cloned into an expression vector, and overexpressed in *E.coli.* The purified enzyme was catalytically active in an aminoacylation assay in which ^{3}H-methionine is incorporated into tRNA (Fig. S2, Supplementary Data). This method uses 100 nM of enzyme to provide an acceptable signal to background ratio which constrains the ability to accurately measure the K_i for highly potent inhibitors (since the IC_{50} can theoretically be no less than half the enzyme concentration). In order to measure the K_i for the MetRS inhibitors, the ATP:PP_i exchange assay was adopted (31). In this method, incorporation of [^{32}P]PP_i into ATP occurs by the reverse enzyme reaction that can be measured when the receiving substrate, tRNA, is omitted. The K_m for the enzyme substrates, methionine and ATP, are within a factor of 2-3 of the values measured in this study and reported elsewhere (31) for the *S. aureus* MetRS. In contrast, the K_m values of methionine and ATP for the human mitochondrial MetRS are lower by a factor of 5-10.

Since the MetRS inhibitors are competitive with methionine (31), it is possible to accurately measure the IC_{50}s of inhibitors in the reaction by raising the concentration of methionine above its K_m (34). The shift in IC_{50} is proportional to the [substrate]/K_m as described by the Cheng-Prusoff equation for competitive inhibitors (35). Of note, the method of raising the methionine substrate concentration cannot be employed in the

aminoacylation assay mentioned earlier because the unlabeled methionine competes with the ^{3}H-methionine that is necessary for the readout. The K_i values were determined for selected MetRS inhibitors revealing extraordinary potency of many of these compounds, ranging from 0.0009 to >1.33 nM (Table 4). This is similar to the K_i for antibiotic MetRS inhibitor, REP8839 against the *S. aureus* MetRS, reported at 0.01 nM (31). The relationship between the K_i and *C. parvum* EC_{50} showed a strong correlation (R^2 = 0.91; P value <0.0001) consistent with the observation that compound **2093** was the most potent compound against the MetRS enzyme and against *C. parvum* infection of cell cultures. The correlation data support the conclusion that the inhibitors act "on target" to mediate their effects on *C. parvum* cells.

More than 500 MetRS inhibitors have been developed in our program to optimize their antitrypanosomal and antibacterial activities (24-26, 30). A set of structurally diverse compounds from this library (Tables 3 and 4) was screened against *C. parvum*, revealing a mix of positive and negative results. The aminoquinolone-containing compounds (exemplified by **1312**, (24)) had poor activity. The aminoquinolone-compounds are in clinical development as antibiotics for *Clostridium difficile* and *S. aureus* infections (36, 37). Similarly, compounds with the urea moiety (e.g. **1433,** (25)) also had poor activity. In contrast, compounds with the fluoro-imidazopyridine (e.g., **1614** and **1717**, (26)) demonstrated more potent activity, in the 5-10 µM range. Parallel work had indicated that changes to the linker region of the molecule were well tolerated, leading to explorations of various changes including ring systems at this region of the molecule (30). Compounds with the 1, 3-dihydro-2-oxo-imidazole as the linker ring were particularly active (Table 4). Among the compounds containing the 1, 3-dihydro-2-oxo-imidazole, various substitutions were explored at the R-groups indicated in Table 4. R_1 as ethyl (e.g., **2062**) was more active than R as H (**1962**) or as propyl (**2069**). R1 as $-CH_2CF_2H$ appears to be slightly less active than the ethyl version. R_2 as F is slightly less active than R_2 as Cl; and Br is essentially the same as Cl. Next, substitutions on the benzyl group (on the left-side of the structure, Table 4) were explored. It had been previously shown that 3, 5-substitutions (such as 3 ,5 -dichlorobenzyl) were particularly potent on the *T. brucei* MetRS (24). In the orientation created by the ring-linker structures, the 2, 4-subsitutions (as shown in Table 4) have the greatest potency. Changing R_4 from Cl to $-OCH_3$, produced the most potent inhibitors in the series (e.g., **2093** and **2114**). Compounds with a tri-substituted benzyl-group (e.g. 2, 4, 5-substitutions) had much diminished activity against *C. parvum* oocysts (data not shown). In summary, compound **2093** was the most potent compound (EC_{50} = 0.007 µM) and compares very favorably to the published data for the clinical drug, nitazoxanide (EC_{50} = 3.7 µM), against *C. parvum* (38).

The activity of the MetRS inhibitors against *C. parvum* infection was tested in two different murine models. The NOD SCID gamma mouse model was performed with a PCR-based readout comparing pre-treatment (day 5) to post-treatment (day 11) fecal

340 parasite levels. Fecal oocysts were significantly reduced for **2093** (tested twice) as well
341 as for **2069** and **2259**, but not for **2067**. The activities were then retested in the
342 *Cryptosporidium* infection model using adult IFN-γ knockout mice. In this model, the
343 mice were monitored for 20 days post-infection. Quantitation of stool parasite loads
344 again showed that **2093** was highly efficacious (>4 $\log_{10}$ drop in luminescence) at the
345 oral dose of 50 mg/kg BID (Fig 3A). The greater magnitude of parasite reduction
346 observed in the IFN-γ knockout mice may be due to differences in the models and
347 readout methods. Additionally, the challenge dose was lower in the IFN-γ knockout
348 mice (10^3) compared to the NSG model (10^5) which may account for the differences if
349 there is an inoculum effect as seen with some bacterial infections (39). A persistence
350 of a low luminescence signal above background levels ($\log_{10}$ RLU of 2.5) was detected
351 during the remainder of the monitoring period in the IFN-γ model, the significance of
352 which is unclear. Importantly, the parasite signal did not rebound to the high levels
353 observed with the controls. Also, the mice maintained their body weight and survived to
354 the end of the 20 day observation period, unlike the vehicle-treated mice that needed to
355 be euthanized on day 17 due to loss of >20% body weight (Fig. 3A). Several follow up
356 experiments confirmed the in vivo activity of **2093** at lower doses (e.g. 50 mg/kg/day
357 divided in one or two doses), but the activity was substantially diminished at the dose of
358 20 mg/kg once per day. The other compounds with excellent in vivo activity were **2114**
359 and **2259**. The mice appeared to tolerate the treatments without any observed side
360 effects, and did not experience the weight loss that was observed in the vehicle-treated
361 mice. The one exception was for **2258** where the mice lost weight and were euthanized
362 on day 13 (before the control mice needed to be euthanized). For the other
363 compounds, it was encouraging to observe that potent anticryptosporidial activity was
364 associated with good clinical outcomes in the mice.
365 The compounds with the greatest in vivo efficacy (**2093**, **2114** and **2259**) were
366 among the most potent in vitro compounds. To further understand the reasons for the
367 more potent in vivo activity, various physicochemical properties were assessed. Some
368 general characteristics of these potent in vivo compounds are molecular weights in the
369 400-450 range, log P in the 3.5-3.75 range, and relatively high solubility (>25 µM) at pH
370 levels reflective of the gastrointestinal tract and plasma. The MetRS inhibitors are all
371 highly protein-bound in the range of 95-99.9% (except for 2240 with 87.7% protein
372 binding). Apparently, high protein binding is not detrimental to activity since compound
373 **2093** is 99.9% bound to mouse plasma proteins. Figure 4 allows for visualization of the
374 chemical properties as they relate to in vivo efficacy. It shows that the most active
375 compounds in vivo have relatively high solubility/EC_{50}, apparently reflecting the
376 importance of in vitro potency (EC_{50}) and, at least, moderate solubility. Interestingly, the
377 most effective compounds had intermediate levels of predicated permeability perhaps
378 suggesting that overly permeable compounds may be completely absorbed into the
379 blood and thus unavailable in the gut for local antiparasitic activity, and that compounds

with low permeability may not cross membranes sufficiently to exert effects on the parasites either.

The liver microsome metabolic half-lives for the MetRS inhibitors were relatively low (<15 min for most compounds tested, Table 6). In fact, the lead compound **2093** has a half-life of 3.2 and 8.3 minutes in murine and human microsomes, respectively. This short in vitro half-life does not directly translate to low plasma exposure in vivo, probably because of the protective effects of the high plasma protein binding.

The pharmacokinetic (PK) properties in mice of several of the MetRS inhibitors were also assessed. The two most potent compounds (**2093** and **2114**) had similar PK profiles with C_{max} in the 6-8 µM range and AUC ~2000 min*umol/L. Fecal levels of **2093** and **2114** were 31 and 11 µM, respectively. The fecal levels suggest that sufficient amounts of intact compound (>100 x EC_{50}) are available in the fecal stream to exert anti-cryptosporidiosis effects. Previous studies with "bumped kinase inhibitors" indicate that intestinal levels of compound better correlate with anti-cryptosporidiosis activity than do plasma levels (12). Both the fecal levels and plasma levels were similar enough amongst the tested *Cp*MetRS inhibitors thus it is not possible to make firm conclusions about the most favorable properties. One exception is that compound **2240** had very high average fecal levels (846 µM) yet had no in vivo anti-*Cryptosporidium* activity. We speculate that this compound may have passed through the GI tract in an insoluble form that was not available for local anti-cryptosporidiosis activity. If this is true then merely delivering insoluble compound to the gut is not sufficient. Since the pathogen lives in an intracellular niche, it is necessary for the compound to be in solution and sufficiently permeable to reach that niche either directly from the intestinal lumen or via the bloodstream.

The safety of the compounds is of great importance given that the target population for anti-cryptosporidiosis treatment will include very young children and other vulnerable groups. A potential concern for MetRS inhibitors is cross-activity on the human mitochondrial MetRS enzyme that could lead to mitochondrial dysfunction. The human mitochondrial MetRS and the *Cp*MetRS are identical at 18 of 25 residues in the compound binding pocket (see Table 1), indicating moderate similarity. An assay was performed to quantify cytochrome oxidase 1 (COX-1) enzyme levels in human liver cells (HepG2) after six-day incubation with MetRS inhibitors. This enzyme is encoded and expressed in the mitochondrion, whereas the control protein (SDH-A) is encoded in the nucleus and expressed in the cytoplasm. The single ring-linker MetRS inhibitors (Table 4), in fact, demonstrated substantial inhibition of COX-1 expression levels with EC_{50} values as low as 0.039 µM in the case of **2093.** This is only slightly above the EC_{50} value against *C. parvum* (0.007 – 0.036 µM). The other single ring-linker compounds generally had EC_{50} values <0.5 µM in this assay. The in vivo effects that may result from mitochondrial protein synthesis inhibition will require further investigation. It is worth noting that many antibiotics that work by inhibiting prokaryotic protein synthesis

420 also inhibit mitochondrial protein synthesis (40). For example, the commonly used
421 antibiotics such as doxycycline (COX-1 EC_{50} = 6.6 µM) and linezolid (COX-1 EC_{50} = 15
422 µM) are used at plasma levels that approximate or exceed the EC_{50} concentrations in
423 the COX-1 assay (41, 42). In the case of linezolid, toxicity due to mitochondrial inhibition
424 can be observed during normal use of the drug, although this typically does not become
425 serious until after four weeks of treatment (43). With anticipated treatment courses for
426 cryptosporidiosis being relatively short (ideally no more than three days), it is likely that
427 brief exposures to MetRS inhibitors would be well tolerated, although clearly this will
428 require careful investigation. If mitochondrial inhibition is a problem, then additional
429 effort to identify more selective compounds will be pursued in future work.
430 The compounds with the best in vivo activity (**2093**, **2114**, and **2259**) were also
431 tested for inhibition of the hERG channels and CYP450 enzymes. The hERG inhibition
432 assay screens for potential of the compound to promote dangerous cardiac
433 dysrhythmias. In the presence of plasma protein (BSA), the percent inhibition was only
434 ~20% at concentrations of 30 µM which is reassuring. The concentration that
435 substantially inhibits hERG channels is likely to be several multiples above the peak
436 concentrations that would occur during treatment. This same compound had little effect
437 on CYP450 enzymes except for CYP2C8 (causing 62-87% inhibition at 10 µM).
438 Common drugs that are metabolized by CYP2C8 include: rosiglitazone (antidiabetic),
439 montelukast (asthma), cerivastatin (statin), and amodiaquine (antimalarial). The co-
440 administration of these MetRS inhibitors with the listed drugs could potentially lead to
441 drug-drug interactions. Finally, Ames and in vitro micronucleus tests were done on
442 compound **2093** and were negative. This provides reassurance that **2093** is not
443 genotoxic.
444 In summary, the imidazopyridine compounds described herein have potent
445 activity against the *C. parvum* MetRS enzyme as well as against cultures of *C. parvum*
446 and *C. hominis.* Parasite persistence assays suggest the compounds have parasiticidal
447 effects on the parasites. Most importantly, the MetRS inhibitors controlled *C. parvum*
448 infection in two murine models without producing side effects. The active compounds
449 demonstrated substantial plasma exposures as well as fecal levels, but it is not entirely
450 clear from these data which of these pharmacological parameters is most relevant. The
451 MetRS inhibitors are capable of inhibiting the human mitochondrial MetRS enzyme as
452 determined by reduced levels of a mitochondrial protein (COX-1) in cultured HepG2
453 cells; however, clinical toxicity may be unlikely if the duration of treatment is kept to
454 short durations (e.g. <1 week). Future studies with **2093** and other MetRS inhibitors in
455 the calf *Cryptosporidium* infection model as well as in vivo toxicology studies will help
456 establish the potential for developing these compounds for treatment of human
457 cryptosporidiosis.
458

459 **METHODS**

Protein sequence alignments: Global pairwise amino acid sequence alignments were generated with the NCBI alignment tool Clustal Omega (44).

***Cp*MetRS cloning, expression, and purification:** The *Cp*MetRS gene (UniProtKB accession number Q5CVN0) was PCR amplified from genomic DNA isolated from the *C. parvum* Iowa II strain. The PCR product was then cloned into the AVA0421 plasmid (45), and the sequence was verified. The expression of the recombinant protein was performed as previously described (45). The protein was purified by nickel affinity chromatography followed by size-exclusion chromatography.

Enzyme assays: Inhibition of *Cp*MetRS was measured using an ATP:PP_i exchange assay as previously described (31, 46) with some modifications. The compounds were pre-incubated for 5 min at room temperature in a 96 well-plate with 30 nM *Cp*MetRS, 125 mM L-methionine, 25 µM $NaPP_i$, ~2 µCi of ^{32}P-tetrasodium pyrophosphate (NEX019001MC, PerkinElmer), 2.5 mM dithiothreitol, 100 mM Tris-HCl pH 8.0, 10 mM magnesium acetate, 80 mM KCl, and 2% dimethyl sulfoxide (DMSO). The reaction was started with the addition of 25 µM ATP, after a 10 min incubation at room temperature, 5 µL of the reaction (in duplicate) was quenched into a $MultiScreen_{HTS}$ Durapore™ 96-well filter plate (MSHVN4B50, Millipore Sigma) containing a mixture of 200 µL of 10% charcoal with 0.5% HCl and 50 µL of 1M HCl with 200 mM of sodium pyrophosphate. The filter plates were washed three times with 200 µL of 1M HCl with 200 mM of sodium pyrophosphate on a vacuum manifold. The plates were dried for 30 minutes at room temperature and then 25 µL of scintillation cocktail was added. Plates were incubated at room temperature for ~1.5 hours before counts per minute (CPM) were quantified on the MicroBeta2 scintillation counter (PerkinElmer). Percent inhibition was calculated by subtracting off the background wells (containing all assay reagents except ATP and compound) and comparing this to the high control wells (containing all assay reagents without compound). IC_{50}s were calculated by non-linear regression methods using the Collaborative Drug Database (Burlingame, CA. www.collaborativedrug.com). K_is were calculated from the IC_{50}s that were shifted above the enzyme concentration (30 nM) using the Cheng-Prusoff equation: $IC_{50} = (1+[Met]/K_m^{Met})(1+K_m^{ATP}/[ATP])K_i$ (31). The K_ms for L-methionine were determined using the same assay conditions above with either *Sa*MetRS or *Cp*MetRS (30 nM) without compounds and with ~5 µCi of ^{32}P-tetrasodium pyrophosphate, 2.5 mM of ATP, and 2.5 mM of $NaPP_i$ while titrating the L-methionine. The reaction was quenched as described above at different time intervals, typically 0, 4, 8, 12, 16, and 20 min. Similarly, the K_ms for ATP were measured by using 1 mM of L-methionine and 2.5 mM of $NaPP_i$ while titrating the ATP. K_m and V_{max} values were calculated in Prism (version 3.0) software. K_{cat} is equal to the V_{max} divided by the enzyme concentration (30 nM).

Chemistry: Compound synthesis for **1312** (24),**1433** (25), **1614** (26), **1717** (26), **1962** (27), **2062** (27), **2093** (27), and **2114** (27) were reported previously. Synthesis of compounds **2067**, **2069**, **2080**, **2091**, **2138**, **2139**, **2207**, **2240**, **2242**, **2258**, and **2259** are described in the supplemental material.

Propogation methods and growth inhibition assays for *C. parvum*: Genetically modified Nanoluciferase (Nluc) expressing *C. parvum* Iowa strain oocysts were propagated in female interferon-γ knockout mice (C57BL/6 IFN-c-deficient mice B6.129S7-Ifngtm1Ts/J, The Jackson Laboratory, Bar Harbor, ME) (47). Mice were infected by oral gavage with 1,000 oocysts in 0.1 mL DPBS (Sigma, St. Louis, MO). Fecal samples were collected starting 3-5 days after infection. Multiple times per week for 2 to 3 weeks, mice were transferred to a clean cage for 1-2 hours, and feces were collected and stored in a 2.5% potassium dichromate solution at 4°C. Oocysts were purified from feces using sucrose flotation followed by cesium chloride gradient as previously described (48).

Growth inhibition assays at University of Washington were performed as follows. HCT-8 cells were added to a 96-well plate and allowed to grow for 72 h to reach 90-100% confluence. Then the media was removed and test compounds were added in serial dilutions prior to the addition of 1,000 oocysts per well in 0.1 mL RPMI-1640 medium supplemented with 10% horse serum and 1% penicillin/streptomycin. Plates were incubated for 72 h and then Nano-Glo® luciferase reagent (Promega, Madison, WI) was added and plates were read on an EnVision Multilabel Plate Reader (Perkin Elmer, Waltham, MA, USA). EC_{50} curves were calculated as previously described using GraphPad Prism version 6.07 (GraphPad Software, La Jolla, CA) (33).

C. parvum growth inhibition assays completed at the University of Vermont were performed as described previously using wild-type *C. parvum* Iowa strain oocysts freshly isolated from calves (purchased from Bunch Grass Farm, Deary, ID) and high content microscopy (32, 38). Excystation of oocysts was induced by treatment with 10 mM hydrochloric acid (10 min at 37°C), followed by exposure to 2 mM sodium taurocholate (Sigma-Aldrich) in PBS for 10 min at 16°C. Excysted oocysts were then added to 95% confluent HCT-8 cell monolayers in 384-well plates (~5,500 oocysts per well). Compounds were added 3 h after infection, and assay plates were incubated for 48 h post-infection at 37°C under 5% CO2. The cell monolayers were then washed three times with PBS containing 111 mM D-galactose, fixed with 4% paraformaldehyde, permeabilized with 0.25% Triton X-100, and blocked overnight with 4% bovine serum albumin (BSA) in PBS. Parasitophorous vacuoles were stained with 1.33 µg/ml of fluorescein-labeled *Vicia villosa* lectin (Vector Laboratories) diluted in 1% BSA in PBS with 0.1% Tween 20 for 1 h at 37°C, followed by the addition of Hoechst 33258 (AnaSpec) at a final concentration of 0.09 mM diluted in water for another 15 min at 37°C. Wells were then washed five times with PBS containing 0.1% Tween 20. A Nikon Eclipse TE2000 epifluorescence microscope with an automated stage was programmed

538 to focus on the center of each well and take a 3-by-3 composite image using an EXi
539 Blue fluorescence microscopy camera (QImaging, Canada) with a 20X objective
540 (numerical aperture, 0.45). Nucleus and parasite images were exported separately as
541 tiff files and were analyzed on the ImageJ platform (National Institutes of Health) using
542 previously developed macros (38).
543 The methods for screening *C. hominis* and clinical isolates of *C. parvum* from
544 dairy calves (reported in supplementary data) were the same as reported previously
545 (49). The strains were collected by Dr. McNamara at CALIBR (32).

546 **Parasite persistence assays:** The procedures were previously published (32). Briefly,
547 HCT-8 cell monolayer infections were established as above in 384-well culture plates
548 using wild-type *C. parvum* Iowa strain oocysts. After approximately 24 h, compounds
549 were added at various concentrations as labeled, and then parasites and host cells
550 were enumerated at multiple time points using immunofluorescence microscopy. Data
551 points are means and standard deviations for 4 culture wells per time point and are
552 representative of 3 independent experiments. The *P* value is the replicates test result
553 (note that a *P* value of ≥0.05 indicates a valid curve fit).

554 **Mammalian cell growth inhibition assays:** Compounds were tested against CRL-
555 8155, human lymphocytic cells, and HepG2, human hepatocellular cells, as previously
556 described (50). Briefly, compounds were incubated with CRL-8155 cells (30,000/well)
557 or HepG2 cells (25,000/well) for 48 hours in 96-well plates and then developed using
558 AlamarBlue® (ThermoFisher Scientific). The EC_{50} values were calculated from percent
559 inhibition by non-linear regression methods using the Collaborative Drug Discovery
560 database (Burlingame, CA. www.collaborativedrug.com) as previously described (50).

561 **MitoBiogenesis™ In-Cell ELISA Colorimetric assay:** 24 hours before adding
562 compounds, 6,000 HepG2 (human hepatocellular) cells were seeded per well into
563 Gibco™ Collagen I, Coated Plate, 96 Well (A1142803,ThermoFisher Scientific) in
564 culture media (50). The next day, the media was removed and compounds were added
565 in culture media. Every 48 hours thereafter during the 6 day incubation period, the
566 media with compounds was replaced with freshly diluted compounds in media. Plates
567 were then fixed with 4% paraformaldehyde and developed using the MitoBiogenesis™
568 In-Cell ELISA Kit (Colorimetric) (ab110217, Abcam) according to the manufacturer's
569 instructions. The EC_{50} values were calculated from the normalized data by non-linear
570 regression methods using the Collaborative Drug Discovery database (Burlingame, CA.
571 www.collaborativedrug.com) or in Prism (version 3.0) software.

572 **Mouse efficacy models:** The efficacy in adult interferon γ (IFN-γ) knockout (KO) mice
573 completed at the University of Washington was carried out as previously described (33)
574 and were approved by the University of Washington Institutional Animal Care and Use
575 Committee. Briefly, female IFN-γ KO mice (B6.129S7-Ifngtm1Ts/J, Jackson

576 Laboratories) aged 8–10 weeks were infected by oral gavage with 1,000
577 Nanoluciferase-tagged *C. parvum* UGA1 oocysts in 0.1 mL of Dulbecco's phosphate-
578 buffered saline. Each experimental group included 3 mice. On day 6 post-infection,
579 mice were administered compounds orally in a formulation of 3% ethanol/7% Tween
580 80/90% saline for 5 days. The fecal samples were collected out to day 20 post infection
581 and luminescences was quantified in Relative Light Units and normalized as previously
582 described (33).
583 All NOD SCID gamma mouse studies were performed in compliance with animal
584 care guidelines and were approved by the University of Vermont Institutional Animal
585 Care and Use Committee. Male NOD SCID gamma mice with normal flora (NOD.Cg-
586 *Prkdc*^{scid} *Il2rg*^{tm1Wjl}/SzJ) (51) were purchased from The Jackson Laboratory (Bar Harbor,
587 ME, USA) and were housed for at least a week for acclimatization. At the age of 4 to 5
588 weeks, mice were infected by oral gavage with 10^5 *C. parvum* Iowa strain oocysts.
589 Treatment was started on day 6 after infection. Mice (4 per experimental group) were
590 treated orally (p.o.) with test compounds at the indicated doses from days 6-10 post-
591 infection. Oocyst shedding in feces was monitored using a previously validated
592 quantitative PCR (qPCR) assay and primers (52).

593 **Measurements of compound solubility:** Two microliters of 20 mM dimethyl sulfoxide
594 stock solution of compound were added to 398 µL of pH = 7.4, 2.0, or 6.5 in PBS buffer.
595 The mixture was vigorously shaken to mix the sample thoroughly, and then the sample
596 was incubated at 25 °C overnight. The mixture was centrifuged at 25 °C for 20 min at
597 15,000xg. The supernatant 100 µL was transferred into another vial and diluted with 100
598 µL CH_3CN. The two-fold diluted supernatant (100 µL) was analyzed by HPLC/ UV
599 system.
600
601 **Measurements of plasma protein binding:** Compound binding to mouse plasma
602 proteins was determined using Rapid Equilibrium Dialysis device (catalog number
603 89809; ThermoFisher Scientific) or 96-well equilibrium dialyzer plates (catalog number
604 SDIS 9610EN; Nest Group, Inc.) or in-house made micro dialysis plates (53) according
605 to published methods (27, 53) and manufacture's instruction (54).

606 **Parallel artificial membrane permeability assay (PAMPA):** The donor well was filled
607 with 200 µL of PRISMA HT buffer (pH 5.0 or pH 7.4, pION inc.) containing 10 µM test
608 compound. The filter on the bottom of each acceptor well was coated with 4 µL of a
609 GIT-0 Lipid Solution (pION, Inc.) and filled with 200 µL of Acceptor Sink Buffer (pION,
610 Inc.). The acceptor filter plate was put on the donor plate and incubated for 3 hours.
611 After the incubation, the amount of test compound in both the donor and acceptor wells
612 was measured by LC-MS/MS to calculate the permeability rate.

613 **Microsome stability assays:** Liver microsomes were purchased from Sekisui
614 XenoTech, LLC (Kansas City, KS, USA). The microsomes (0.2 mg protein/mL) and the
615 compound (1 µM) were mixed in phosphate buffer (pH 7.4). The reactions were initiated

616 by adding an NADPH generating system (a mixture of MgCl2, β-NADP+, glucose-6-
617 phosphate, and glucose-6-phosphate dehydrogenase) to the mixtures before
618 incubation. Incubations were conducted at 37ºC and terminated by adding acetonitrile.
619 The zero-time incubations, which served as the controls, were terminated by adding
620 acetonitrile before adding an NADPH generating system. After the samples were mixed
621 and centrifuged, the compound concentration in the supernatant fractions were
622 measured by LC/MS/MS. Control compounds demonstrated the following in vitro
623 clearance rates: flutamide: 161 µL/min/mg (human) and 304 µL/min/mg (mouse);
624 quinidine: 4 µL/min/mg (human) and 27 µL/min/mg (mouse); and cilostazol: 28
625 µL/min/mg (human) and 100 µL/min/mg (mouse);

626

627 **CYP450 Inhibition assays:** Human liver microsomes were purchased from Sekisui
628 XenoTech, LLC (Kansas City, KS, USA). The microsomes (0.1 mg protein/mL),
629 substrates (tacrine, paclitaxel, tolbutamide, dextromethorphan, and midazolam) and the
630 compound (10 µM) were mixed in phosphate buffer (pH 7.4). The reactions were
631 initiated by adding an NADPH generating system (a mixture of MgCl2, β-NADP+,
632 glucose-6-phosphate, and glucose-6-phosphate dehydrogenase) to the mixtures before
633 incubation. Incubations were conducted at 37°C for 10 minutes and terminated by
634 adding acetonitrile. The activities of CYP1A2, CYP2C8, CYP2C9, CYP2D6 and
635 CYP3A4 were determined by the peak of 1-hydroxytacrine, 6α-hydroxypaclitaxel, 4-
636 hydroxytolbutamide, dextrorphan and 1'-hydroxymidazolam, respectively. The activities
637 of test samples were expressed as the percentage of activity remaining compared with
638 a control sample containing no inhibitor.

639 **hERG inhibition assays:** hERG/CHO cells stably expressing hERG channel were
640 purchased from Millipore, Ltd (UK). Cells were cultured at 32 ºC, 5% CO2 in Ham's F-
641 12 medium supplemented with 10% fetal bovine serum, 500ug/mL Geneticin . The
642 hERG inhibition assay was performed on the IonWorks Quattro (Molecular Devices)
643 system in population patch clamp (PPC) mode. The extracellular solution was
644 phosphate-buffered saline with calcium and magnesium. The intracellular solution
645 contained 120 µM amphotericin B, 140 mM KCl, 2 mM MgCl2, 1 mM EGTA and 20 mM
646 HEPES (pH 7.3). The hERG current was measured under the potential-clamp protocol
647 (Holding potential -80 mV, the first voltage 40 mV for 2 sec, the second voltage -50 mV
648 for 2 sec). After patch perforation, the peak tail current before addition of the
649 compounds were measured as the pre-hERG current. Test compounds were incubated
650 on the cells for a period of 5 min. The peak tail current after addition of the
651 compounds were measured as the post-hERG current. The hERG inhibition assays
652 were performed in triplicate in two kinds of extracellular solutions which contained 1%
653 BSA or none.

654 **Mouse pharmacokinetics:** Nonfasted female Swiss Webster mice (n=3) were
655 administered 50 mpk of compound by oral gavage in a vehicle consisting of 7% Tween
656 80, 3% ethanol, 5% DMSO, and 0.9% saline. Tail blood was collected at 30, 60, 120,
657 240, 360, 480, and 1,440 min into heparinized capillary tubes and spotted onto
658 Whatman Gel Blotting paper as previously described (50). Whole-blood samples were
659 extracted with acetonitrile and analyzed by liquid chromatography-tandem mass
660 spectrometry. The values of the pharmacokinetic parameters were calculated using
661 Phoenix WinNonlin (version 6.3) software (Certara, Princeton, NJ).

662 Feces were collected and pooled from all three mice from the entire duration of the
663 pharmacokinetic experiment described above (0 min to 1,440 min). The pellets were
664 suspended in 4x water by weight and homogenized. To extract compounds of interest,
665 acetonitrile (8x by volume) was added to the homogenate containing 100 mg of feces
666 followed by addition of internal standard solution (90% acetonitrile : 10% water). After
667 centrifuging the homogenate solution, the supernatant was dried in a speed-vac. The
668 dried samples were reconstituted in a LC-MS sample solution (50% MQ water : 50%
669 Acetonitrile). The solution was centrifuged and the supernatant was transferred to a
670 liquid chromatography insert. Each compound was tested in triplicate. Similarly, fecal
671 homogenate from vehicle mice were prepared to make calibration standards. The
672 compound concentrations for calibration standards were 0 nM, 10 nM, 100 nM, 1 µM, 5
673 µM, 10 µM, 20 µM, 40 µM. The compound concentrations for each homogenate from
674 treated mice group were calculated from the calibration curves using Microsoft Excel
675 software.

676

ACKNOWLEDGEMENTS: Support for this project was provided by PATH with funding from the UK government, and by the National Institutes of Health (grant AI097177). The purified recombinant *C. parvum* MetRS protein (UniProt Q5CVN0) described herein was provided by the Seattle Structural Genomics Center for Infectious Disease (www.SSGCID.org) supported by Federal Contract No. HHSN272201700059C from the National Institute of Allergy and Infectious Diseases, National Institutes of Health, Department of Health and Human Services. We acknowledge the contributions of the following individuals: Nora Molasky, Uyen Nguyen, and Omeed Faghih for performing mammalian cell cytotoxicity assays; Molly McCloskey and Grant Whitman for assisting with in vivo efficacy experiments; Zack Herbst for analytical chemistry on pharmacokinetic assays; and Hannah Udell for cloning and purifying the *C. parvum* MetRS enzyme. We acknowledge contributions of project oversight by Eugenio de Hostos (PATH). We also acknowledge valuable contributions by collaborating scientists at Takeda (Yasushi Miyazaki) and CALIBR (Melissa Love and Case McNamara).

REFERENCES

1. Nations U. https://www.un.org/sustainabledevelopment/sustainable-development-goals/. Accessed
2. Organization WH. 2018. Global Health Estimates 2016: Deaths by Cause, Age, Sex, by Country and by Region, 2000-2016. . World Health Organization, Geneva.
3. Kotloff KL, Nataro JP, Blackwelder WC, Nasrin D, Farag TH, Panchalingam S, Wu Y, Sow SO, Sur D, Breiman RF, Faruque AS, Zaidi AK, Saha D, Alonso PL, Tamboura B, Sanogo D, Onwuchekwa U, Manna B, Ramamurthy T, Kanungo S, Ochieng JB, Omore R, Oundo JO, Hossain A, Das SK, Ahmed S, Qureshi S, Quadri F, Adegbola RA, Antonio M, Hossain MJ, Akinsola A, Mandomando I, Nhampossa T, Acacio S, Biswas K, O'Reilly CE, Mintz ED, Berkeley LY, Muhsen K, Sommerfelt H, Robins-Browne RM, Levine MM. 2013. Burden and aetiology of diarrhoeal disease in infants and young children in developing countries (the Global Enteric Multicenter Study, GEMS): a prospective, case-control study. Lancet 382:209-22.
4. Platts-Mills JA, Babji S, Bodhidatta L, Gratz J, Haque R, Havt A, McCormick BJ, McGrath M, Olortegui MP, Samie A, Shakoor S, Mondal D, Lima IF, Hariraju D, Rayamajhi BB, Qureshi S, Kabir F, Yori PP, Mufamadi B, Amour C, Carreon JD, Richard SA, Lang D, Bessong P, Mduma E, Ahmed T, Lima AA, Mason CJ, Zaidi AK, Bhutta ZA, Kosek M, Guerrant RL, Gottlieb M, Miller M, Kang G, Houpt ER, Investigators M-EN. 2015. Pathogen-specific burdens of community diarrhoea in developing countries: a multisite birth cohort study (MAL-ED). Lancet Glob Health 3:e564-75.
5. Korpe PS, Haque R, Gilchrist C, Valencia C, Niu F, Lu M, Ma JZ, Petri SE, Reichman D, Kabir M, Duggal P, Petri WA, Jr. 2016. Natural History of Cryptosporidiosis in a Longitudinal Study of Slum-Dwelling Bangladeshi Children: Association with Severe Malnutrition. PLoS Negl Trop Dis 10:e0004564.
6. Khalil IA, Troeger C, Rao PC, Blacker BF, Brown A, Brewer TG, Colombara DV, De Hostos EL, Engmann C, Guerrant RL, Haque R, Houpt ER, Kang G, Korpe PS, Kotloff KL, Lima AAM, Petri WA, Jr., Platts-Mills JA, Shoultz DA, Forouzanfar MH, Hay SI, Reiner RC, Jr., Mokdad AH. 2018. Morbidity, mortality, and long-term consequences associated with diarrhoea from

720 Cryptosporidium infection in children younger than 5 years: a meta-analyses study. Lancet Glob
721 Health 6:e758-e768.
722 7. Checkley W, White AC, Jr., Jaganath D, Arrowood MJ, Chalmers RM, Chen XM, Fayer R, Griffiths
723 JK, Guerrant RL, Hedstrom L, Huston CD, Kotloff KL, Kang G, Mead JR, Miller M, Petri WA, Jr.,
724 Priest JW, Roos DS, Striepen B, Thompson RC, Ward HD, Van Voorhis WA, Xiao L, Zhu G, Houpt
725 ER. 2015. A review of the global burden, novel diagnostics, therapeutics, and vaccine targets for
726 cryptosporidium. Lancet Infect Dis 15:85-94.
727 8. Clode PL, Koh WH, Thompson RCA. 2015. Life without a Host Cell: What is Cryptosporidium?
728 Trends Parasitol 31:614-624.
729 9. Shrivastava AK, Kumar S, Smith WA, Sahu PS. 2017. Revisiting the global problem of
730 cryptosporidiosis and recommendations. Trop Parasitol 7:8-17.
731 10. Mor SM, Tumwine JK, Ndeezi G, Srinivasan MG, Kaddu-Mulindwa DH, Tzipori S, Griffiths JK.
732 2010. Respiratory cryptosporidiosis in HIV-seronegative children in Uganda: potential for
733 respiratory transmission. Clin Infect Dis 50:1366-72.
734 11. Mor SM, Ascolillo LR, Nakato R, Ndeezi G, Tumwine JK, Okwera A, Sponseller JK, Tzipori S,
735 Griffiths JK. 2018. Expectoration of Cryptosporidium Parasites in Sputum of Human
736 Immunodeficiency Virus-Positive and -Negative Adults. Am J Trop Med Hyg 98:1086-1090.
737 12. Arnold SLM, Choi R, Hulverson MA, Schaefer DA, Vinayak S, Vidadala RSR, McCloskey MC,
738 Whitman GR, Huang W, Barrett LK, Ojo KK, Fan E, Maly DJ, Riggs MW, Striepen B, Van Voorhis
739 WC. 2017. Necessity of Bumped Kinase Inhibitor Gastrointestinal Exposure in Treating
740 Cryptosporidium Infection. J Infect Dis 216:55-63.
741 13. Nakama T, Nureki O, Yokoyama S. 2001. Structural basis for the recognition of isoleucyl-
742 adenylate and an antibiotic, mupirocin, by isoleucyl-tRNA synthetase. J Biol Chem 276:47387-
743 47393.
744 14. Rock FL, Mao W, Yaremchuk A, Tukalo M, Crepin T, Zhou H, Zhang YK, Hernandez V, Akama T,
745 Baker SJ, Plattner JJ, Shapiro L, Martinis SA, Benkovic SJ, Cusack S, Alley MR. 2007. An antifungal
746 agent inhibits an aminoacyl-tRNA synthetase by trapping tRNA in the editing site. Science
747 316:1759-1761.
748 15. Elewski BE, Aly R, Baldwin SL, Gonzalez Soto RF, Rich P, Weisfeld M, Wiltz H, Zane LT, Pollak R.
749 2015. Efficacy and safety of tavaborole topical solution, 5%, a novel boron-based antifungal
750 agent, for the treatment of toenail onychomycosis: Results from 2 randomized phase-III studies.
751 J Am Acad Dermatol 73:62-9.
752 16. Keller TL, Zocco D, Sundrud MS, Hendrick M, Edenius M, Yum J, Kim YJ, Lee HK, Cortese JF, Wirth
753 DF, Dignam JD, Rao A, Yeo CY, Mazitschek R, Whitman M. 2012. Halofuginone and other
754 febrifugine derivatives inhibit prolyl-tRNA synthetase. Nat Chem Biol 8:311-317.
755 17. O'Dwyer K, Spivak AT, Ingraham K, Min S, Holmes DJ, Jakielaszek C, Rittenhouse S, Kwan AL, Livi
756 GP, Sathe G, Thomas E, Van HS, Miller LA, Twynholm M, Tomayko J, Dalessandro M, Caltabiano
757 M, Scangarella-Oman NE, Brown JR. 2015. Bacterial resistance to leucyl-tRNA synthetase
758 inhibitor GSK2251052 develops during treatment of complicated urinary tract infections.
759 Antimicrob Agents Chemother 59:289-298.
760 18. Hernandez V, Crepin T, Palencia A, Cusack S, Akama T, Baker SJ, Bu W, Feng L, Freund YR, Liu L,
761 Meewan M, Mohan M, Mao W, Rock FL, Sexton H, Sheoran A, Zhang Y, Zhang YK, Zhou Y,
762 Nieman JA, Anugula MR, Keramane el M, Savariraj K, Reddy DS, Sharma R, Subedi R, Singh R,
763 O'Leary A, Simon NL, De Marsh PL, Mushtaq S, Warner M, Livermore DM, Alley MR, Plattner JJ.
764 2013. Discovery of a novel class of boron-based antibacterials with activity against gram-
765 negative bacteria. Antimicrob Agents Chemother 57:1394-403.
766 19. Li X, Hernandez V, Rock FL, Choi W, Mak YSL, Mohan M, Mao W, Zhou Y, Easom EE, Plattner JJ,
767 Zou W, Perez-Herran E, Giordano I, Mendoza-Losana A, Alemparte C, Rullas J, Angulo-Barturen I,

768 Crouch S, Ortega F, Barros D, Alley MRK. 2017. Discovery of a Potent and Specific M.
769 tuberculosis Leucyl-tRNA Synthetase Inhibitor: (S)-3-(Aminomethyl)-4-chloro-7-(2-
770 hydroxyethoxy)benzo[c][1,2]oxaborol-1(3H)-ol (GSK656). J Med Chem 60:8011-8026.
771 20. Palencia A, Li X, Bu W, Choi W, Ding CZ, Easom EE, Feng L, Hernandez V, Houston P, Liu L,
772 Meewan M, Mohan M, Rock FL, Sexton H, Zhang S, Zhou Y, Wan B, Wang Y, Franzblau SG,
773 Woolhiser L, Gruppo V, Lenaerts AJ, O'Malley T, Parish T, Cooper CB, Waters MG, Ma Z, Ioerger
774 TR, Sacchettini JC, Rullas J, Angulo-Barturen I, Perez-Herran E, Mendoza A, Barros D, Cusack S,
775 Plattner JJ, Alley MR. 2016. Discovery of Novel Oral Protein Synthesis Inhibitors of
776 Mycobacterium tuberculosis That Target Leucyl-tRNA Synthetase. Antimicrob Agents Chemother
777 60:6271-80.
778 21. Pham JS, Dawson KL, Jackson KE, Lim EE, Pasaje CF, Turner KE, Ralph SA. 2014. Aminoacyl-tRNA
779 synthetases as drug targets in eukaryotic parasites. Int J Parasitol Drugs Drug Resist 4:1-13.
780 22. Palencia A, Liu RJ, Lukarska M, Gut J, Bougdour A, Touquet B, Wang ED, Li X, Alley MR, Freund
781 YR, Rosenthal PJ, Hakimi MA, Cusack S. 2016. Cryptosporidium and Toxoplasma Parasites Are
782 Inhibited by a Benzoxaborole Targeting Leucyl-tRNA Synthetase. Antimicrob Agents Chemother
783 60:5817-27.
784 23. Gentry DR, Ingraham KA, Stanhope MJ, Rittenhouse S, Jarvest RL, O'Hanlon PJ, Brown JR,
785 Holmes DJ. 2003. Variable sensitivity to bacterial methionyl-tRNA synthetase inhibitors reveals
786 subpopulations of Streptococcus pneumoniae with two distinct methionyl-tRNA synthetase
787 genes. Antimicrob Agents Chemother 47:1784-1789.
788 24. Shibata S, Gillespie JR, Kelley AM, Napuli AJ, Zhang Z, Kovzun KV, Pefley RM, Lam J, Zucker FH,
789 Van Voorhis WC, Merritt EA, Hol WG, Verlinde CL, Fan E, Buckner FS. 2011. Selective Inhibitors
790 of Methionyl-tRNA Synthetase Have Potent Activity against Trypanosoma brucei Infection in
791 Mice. Antimicrob Agents Chemother 55:1982-1989.
792 25. Shibata S, Gillespie JR, Ranade RM, Koh CY, Kim JE, Laydbak JU, Zucker FH, Hol WG, Verlinde CL,
793 Buckner FS, Fan E. 2012. Urea-based inhibitors of Trypanosoma brucei methionyl-tRNA
794 synthetase: selectivity and in vivo characterization. J Med Chem 55:6342-6351.
795 26. Zhang Z, Koh CY, Ranade RM, Shibata S, Gillespie JR, Hulverson MA, Nguyen J, Pendem N, Gelb
796 MH, Verlinde CL, Hol WG, Buckner FS, Fan E. 2016. 5-Fluoro-imidazo[4,5-b]pyridine is a
797 privileged fragment that conveys bioavailability to potent trypanosomal methionyl-tRNA
798 synthetase inhibitors. ACS Infect Dis 2:399-404.
799 27. Faghih O, Zhang Z, Ranade RM, Gillespie JR, Creason SA, Huang W, Shibata S, Barros-Alvarez X,
800 Verlinde C, Hol WGJ, Fan E, Buckner FS. 2017. Development of Methionyl-tRNA Synthetase
801 Inhibitors as Antibiotics for Gram-Positive Bacterial Infections. Antimicrob Agents Chemother
802 61.
803 28. Koh CY, Kim JE, Shibata S, Ranade RM, Yu M, Liu J, Gillespie JR, Buckner FS, Verlinde CL, Fan E,
804 Hol WG. 2012. Distinct States of Methionyl-tRNA Synthetase Indicate Inhibitor Binding by
805 Conformational Selection. Structure 20:1681-1691.
806 29. Koh CY, Kim JE, Wetzel AB, WJ dvdS, Shibata S, Ranade RM, Liu J, Zhang Z, Gillespie JR, Buckner
807 FS, Verlinde CL, Fan E, Hol WG. 2014. Structures of Trypanosoma brucei methionyl-tRNA
808 synthetase with urea-based inhibitors provide guidance for drug design against sleeping
809 sickness. PLoS Negl Trop Dis 8:e2775.
810 30. Huang W, Zhang Z, Barros-Alvarez X, Koh CY, Ranade RM, Gillespie JR, Creason SA, Shibata S,
811 Verlinde CL, Hol WG, Buckner FS, Fan E. 2016. Structure-guided design of novel Trypanosoma
812 brucei Methionyl-tRNA synthetase inhibitors. Eur J Med Chem 124:1081-1092.
813 31. Green LS, Bullard JM, Ribble W, Dean F, Ayers DF, Ochsner UA, Janjic N, Jarvis TC. 2009.
814 Inhibition of methionyl-tRNA synthetase by REP8839 and effects of resistance mutations on
815 enzyme activity. Antimicrob Agents Chemother 53:86-94.

816 32. Jumani RS, Bessoff K, Love MS, Miller P, Stebbins EE, Teixeira JE, Campbell MA, Meyers MJ,
817 Zambriski JA, Nunez V, Woods AK, McNamara CW, Huston CD. 2018. A Novel Piperazine-Based
818 Drug Lead for Cryptosporidiosis from the Medicines for Malaria Venture Open-Access Malaria
819 Box. Antimicrob Agents Chemother 62.
820 33. Hulverson MA, Vinayak S, Choi R, Schaefer DA, Castellanos-Gonzalez A, Vidadala RSR, Brooks CF,
821 Herbert GT, Betzer DP, Whitman GR, Sparks HN, Arnold SLM, Rivas KL, Barrett LK, White AC, Jr.,
822 Maly DJ, Riggs MW, Striepen B, Van Voorhis WC, Ojo KK. 2017. Bumped-Kinase Inhibitors for
823 Cryptosporidiosis Therapy. J Infect Dis 215:1275-1284.
824 34. Pope AJ, Moore KJ, McVey M, Mensah L, Benson N, Osbourne N, Broom N, Brown MJ, O'Hanlon
825 P. 1998. Characterization of isoleucyl-tRNA synthetase from Staphylococcus aureus. II.
826 Mechanism of inhibition by reaction intermediate and pseudomonic acid analogues studied
827 using transient and steady-state kinetics. J Biol Chem 273:31691-701.
828 35. Cheng Y, Prusoff WH. 1973. Relationship between the inhibition constant (K1) and the
829 concentration of inhibitor which causes 50 per cent inhibition (I50) of an enzymatic reaction.
830 Biochem Pharmacol 22:3099-108.
831 36. Critchley IA, Ochsner UA. 2008. Recent advances in the preclinical evaluation of the topical
832 antibacterial agent REP8839. Curr Opin Chem Biol 12:409-417.
833 37. Critchley IA, Green LS, Young CL, Bullard JM, Evans RJ, Price M, Jarvis TC, Guiles JW, Janjic N,
834 Ochsner UA. 2009. Spectrum of activity and mode of action of REP3123, a new antibiotic to treat
835 Clostridium difficile infections. J Antimicrob Chemother 63:954-963.
836 38. Bessoff K, Sateriale A, Lee KK, Huston CD. 2013. Drug repurposing screen reveals FDA-approved
837 inhibitors of human HMG-CoA reductase and isoprenoid synthesis that block Cryptosporidium
838 parvum growth. Antimicrob Agents Chemother 57:1804-14.
839 39. Soriano F, Santamaria M, Ponte C, Castilla C, Fernandez-Roblas R. 1988. In vivo significance of
840 the inoculum effect of antibiotics on Escherichia coli. Eur J Clin Microbiol Infect Dis 7:410-2.
841 40. Cohen BH, Saneto RP. 2012. Mitochondrial translational inhibitors in the pharmacopeia. Biochim
842 Biophys Acta 1819:1067-1074.
843 41. Ribes S, Pachon-Ibanez ME, Dominguez MA, Fernandez R, Tubau F, Ariza J, Gudiol F, Cabellos C.
844 2010. In vitro and in vivo activities of linezolid alone and combined with vancomycin and
845 imipenem against Staphylococcus aureus with reduced susceptibility to glycopeptides. Eur J Clin
846 Microbiol Infect Dis 29:1361-7.
847 42. Newton PN, Chaulet JF, Brockman A, Chierakul W, Dondorp A, Ruangveerayuth R, Looareesuwan
848 S, Mounier C, White NJ. 2005. Pharmacokinetics of oral doxycycline during combination
849 treatment of severe falciparum malaria. Antimicrob Agents Chemother 49:1622-5.
850 43. Garrabou G, Soriano A, Lopez S, Guallar JP, Giralt M, Villarroya F, Martinez JA, Casademont J,
851 Cardellach F, Mensa J, Miro O. 2007. Reversible inhibition of mitochondrial protein synthesis
852 during linezolid-related hyperlactatemia. Antimicrob Agents Chemother 51:962-967.
853 44. Sievers F, Wilm A, Dineen D, Gibson TJ, Karplus K, Li W, Lopez R, McWilliam H, Remmert M,
854 Soding J, Thompson JD, Higgins DG. 2011. Fast, scalable generation of high-quality protein
855 multiple sequence alignments using Clustal Omega. Mol Syst Biol 7:539.
856 45. Choi R, Kelley A, Leibly D, Hewitt SN, Napuli A, Van Voorhis W. 2011. Immobilized metal-affinity
857 chromatography protein-recovery screening is predictive of crystallographic structure success.
858 Acta Crystallogr Sect F Struct Biol Cryst Commun 67:998-1005.
859 46. Beebe K, Waas W, Druzina Z, Guo M, Schimmel P. 2007. A universal plate format for increased
860 throughput of assays that monitor multiple aminoacyl transfer RNA synthetase activities. Anal
861 Biochem 368:111-121.

862 47. Vinayak S, Pawlowic MC, Sateriale A, Brooks CF, Studstill CJ, Bar-Peled Y, Cipriano MJ, Striepen B.
863 2015. Genetic modification of the diarrhoeal pathogen Cryptosporidium parvum. Nature
864 523:477-80.
865 48. Arrowood MJ, Donaldson K. 1996. Improved purification methods for calf-derived
866 Cryptosporidium parvum oocysts using discontinuous sucrose and cesium chloride gradients. J
867 Eukaryot Microbiol 43:89S.
868 49. Love MS, Beasley FC, Jumani RS, Wright TM, Chatterjee AK, Huston CD, Schultz PG, McNamara
869 CW. 2017. A high-throughput phenotypic screen identifies clofazimine as a potential treatment
870 for cryptosporidiosis. PLoS Negl Trop Dis 11:e0005373.
871 50. Silva DG, J.R.; Ranade, Ranae; Herbst, Zackary; Nguyen, Uyen; Buckner, F.S.; Montanari, Carlos;
872 Gelb, Michael. 2017. A New Class of Antitrypanosomal Agents Based on Imidazopyridines. ACS
873 Med Chem Lett.
874 51. Shultz LD, Lyons BL, Burzenski LM, Gott B, Chen X, Chaleff S, Kotb M, Gillies SD, King M,
875 Mangada J, Greiner DL, Handgretinger R. 2005. Human lymphoid and myeloid cell development
876 in NOD/LtSz-scid IL2R gamma null mice engrafted with mobilized human hemopoietic stem cells.
877 J Immunol 174:6477-89.
878 52. Parr JB, Sevilleja JE, Samie A, Alcantara C, Stroup SE, Kohli A, Fayer R, Lima AA, Houpt ER,
879 Guerrant RL. 2007. Detection and quantification of Cryptosporidium in HCT-8 cells and human
880 fecal specimens using real-time polymerase chain reaction. Am J Trop Med Hyg 76:938-42.
881 53. Herbst ZM, Shibata S, Fan E, Gelb MH. 2018. An Inexpensive, In-House-Made, Microdialysis
882 Device for Measuring Drug-Protein Binding. ACS Med Chem Lett 9:279-282.
883 54. Scientific T. https://assets.thermofisher.com/TFS-
884 Assets/LSG/manuals/MAN0011619_SgleUse_RED_Plate_Insert_UG.pdf. Accessed
885 55. Spencer AC, Heck A, Takeuchi N, Watanabe K, Spremulli LL. 2004. Characterization of the human
886 mitochondrial methionyl-tRNA synthetase. Biochemistry 43:9743-9754.

887

Table 1. Protein sequence analysis of MetRS inhibitor-binding sites from different species[a]

	Zone, pocket, or amino acid by sequence number[b]																							
Pocket or species	247	248	249	250	287	289	290	291	292	456	460	461	470	471	472	473	474	476	477	478	480	481	519	522	523
Pocket	b	b	b	l	q	q	q	q	q	q	q	q	q	q	q	q	b	q	b	b	b	b	b	b	b
Trypanosoma brucei	Pro	Ile	Tyr	Tyr	Asp	His	Gly	Gln	Lys	Leu	Ala	Ile	Cys	Val	Tyr	Val	Trp	Asp	Ala	Leu	Asn	Tyr	Ile	Phe	His
Cryptosporidium parvum/hominis	Ala	Ile	Tyr	Tyr	Asp	His	Gly	Gln	Lys	Ala	Gly	Val	Val	Met	Tyr	Val	Trp	Asp	Ala	Leu	Asn	Tyr	Ile	Phe	His
Homo sapiens (mitochondrial)	Pro	Ile	Phe	Tyr	Asp	His	Gly	Leu	Lys	¶	Gly	Ile	Thr	Ile	Tyr	Val	Trp	Asp	Ala	Leu	Asn	Tyr	Ile	Phe	His
Homo sapiens (cytoplasmic)	Ala	Leu	Pro	Tyr	Asp	Tyr	Gly	Thr	Ala	¶	Gly	Thr	Val	Phe	Tyr	Val	Trp	Asp	Ala	Thr	Gly	Tyr	Asn	Phe	His

[a] Sequence #s refer to the *T. brucei* sequence. UNIPROT accession codes: *T. brucei* - Q38C91; *C. parvum* – Q5CVN0; *C. hominis* – UPI0000452AB0; *H. sapiens*/mito - Q96GW9; *H. sapiens*/cyto - P56192.

[b] *l* = linker zone, *b* = benzyl pocket (methionine substrate pocket), *q* = quinolone pocket (auxiliary pocket formed upon inhibitor binding) .

¶ Ambiguous: due to different loop length could be Leu or His.

Table 2. Kinetic parameters of *C. parvum* MetRS compared to MetRS enzymes from other organisms

	Met			ATP			Reference
MetRS	K_m (μM)	K_{cat} (S^{-1})	K_{cat}/K_m($\mu M^{-1}S^{-1}$)	K_m (μM))	K_{cat} (S^{-1})	K_{cat}/K_m($\mu M^{-1}S^{-1}$)	
C. parvum	71	37	0.52	1040	33	0.03	This work
S.aureus	77	36	0.47	347	26	0.07	This work
S.aureus	100	25	0.25	500	25	0.05	(31)
Human mitoch	18	0.41	0.023	85	0.033	0.00038	(55)

Table 3. Activities of MetRS inhibitors with linear linkers (mean ± SD)

Molecule Name	Structure	*C. parvum* MetRS Ki (nM)	UW *C. parvum* EC50 (μM)	U. VT *C. parvum* EC50 (μM)	COX-1 EC50 (μM)	SDH-A EC50 (μM)	CRL-8155 EC50 (μM)*	Hep G2 EC50 (μM)*	Reference
1312	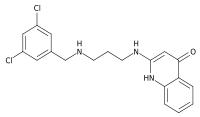	0.64 ± 0.01 (n=2)	18.55 ± 0.212 (n=2)	> 10.0; > 50.0	2.43	>25	> 20.0	> 20.0	(24)
1433	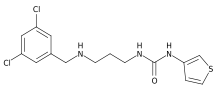	> 1.33 (n =2)	> 20.00 ± 0.000 (n=2)	> 10.0, 11.2	14.7	12.2	14 ± 2.8 (n=2)	16.5 ± 4.9 (n=2)	(25)
1614	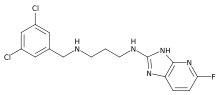	0.61 ± 0.06 (n=2)	14.80 ± 2.404 (n=2)	7.60 ± 0.74 (n=2)	4.35 ± 0.92 (n=2)	31.5 ± 2.1 (n=2)	39.7 ± 0.8 (n=2)	> 50.0	(26)
1717	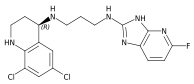	0.41 ± 0.06 (n=2)	4.10 ± 2.59 (n=2)	5.17 ± 0.45 (n=2)	1.04 ± 0.51 (n=2)	>25 (n=2)	14.1 ± 9.5 (n=5)	25.4 ± 8.4 (n=4)	(26)
1369 bumped kinase inhibitor (Reference standard)	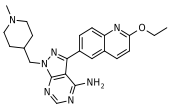	Not applicable	2.4 ± 0.7 (n=2)	Not done	Not applicable	Not applicable	>40.0	>40.0	(33)

*Cytotoxicity data previously published for **1312** (24), **1614** (26),**1717** (26), and **1369** (33)
Reference standard for CRL-8155 cells: Quinacrine EC_{50} = 3.99 ± 2.27 µM (n=14)
Reference standard for HepG2 cells: Quinacrine EC_{50} = 9.76 ± 2.73 µM (n=13)
Reference standard for COX-1: Chloramphenicol EC_{50} = 6.31 ± 0.91 (n=8)
Reference standard for SDH-A: Chloramphenicol EC_{50} = >50 ± 0 (n=8)

907 **Table 4. Activities of MetRS inhibitors with a single ring in the linker (mean ± SD)**

908 **MetRS inhibitor scaffold**

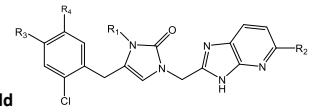

Cmpd 2242

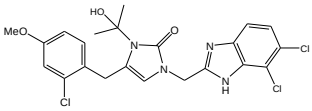

Molecule Name	R1	R2	R3	R4	*C. parvum* MetRS Ki (nM)	UW *C. parvum* EC50 (μM)	U. VT *C. parvum* EC50 (μM)	COX-1 EC50 (μM)	SDH-A EC50 (μM)	CRL-8155 EC50 (μM)*	Hep G2 EC50 (μM)*	Reference
1962	H	F	Cl	H	> 1.33 (n=2)	>20.000 ± 0.000 (n=2)	8.48 ± 0.81 (n=2)	>25	>25	>50.0	>50.0	(27)
2062	$-CH_2-CH_3$	F	Cl	H	0.0162 ± 0.0017 (n=2)	1.865 ± 0.884 (n=2)	0.152 (n=2)	0.29	>25	>50.0	>50.0	(27)
2114	$-CH_2-CH_3$	F	$-OCH_3$	H	0.0023 +/- 0.0011 (n=3)	0.060 ± 0.011 (n=2)		0.075	>25	>50.0	>50.0	(27)
2067	$-CH_2-CH_3$	Cl	Cl	H	0.0093 ± 0.0002 (n=2)	0.408 ± 0.286 (n=2)	0.076 (n=2)	0.042	>25	>50.0	>50.0	This work
2091	$-CH_2-CH_3$	Br	Cl	H		0.598 (n=1)	0.376 (n=2)			>50.0	>50.0	This work
2093	$-CH_2-CH_3$	Cl	$-OCH_3$	H	0.0009 +/- 0.0004 (n=12)	0.036 ± 0.004 (n=2)	0.007 (n=2)	0.039	>25	>50.0	>50.0	(27)
2069	$-CH_2-CH_2-CH_3$	F	Cl	H	0.016 +/- 0.010 (n=3)	0.411 ± 0.266 (n=2)	0.043 (n=2)	0.195	>25	>50.0	>50.0	This work
2139	$-CH_2-CF_2H$	F	Cl	H	0.066 +/- 0.022 (n=2)	0.284 ± 0.128 (n=2)		0.175	>25	33.3	>50.0	This work

2259	$-CH_2-CF_2H$	F	$-OCH_3$	H	0.0038 +/- 0.0014 (n=3)	0.134 ± 0.089 (n=2)		0.164	>25	>50.0	>50.0	This work
2138	$-CH_2-CF_2H$	Cl	Cl	H	0.0187 +/- 0.0004 (n=2)	0.454 ± 0.252 (n=2)	0.416 ± 0.127 (n=2)	0.430	>25	>50.0	>50.0	This work
2258	$-CH_2-CF_2H$	Cl	$-OCH_3$	H	0.0036 +/- 0.0019 (n=3)	0.19 ± 0.004 (n=2)		0.134	>25	>50.0	>50.0	This work
2207	$-CH_2-C(CH_3)_2OH$	Cl	Cl	H		0.129 (n=1)	0.100 ± 0.019 (n=2)	0.055	>25	>50.0	>50.0	This work
2240	$-CH_2-C(CH_3)_2OH$	Cl	$-OCH_3$	$-OCH_3$		0.31 ± 0.170 (n=2)				>50.0	>50.0	This work
2080	$-CH(CH_3)_2$	F	Cl	H		0.52 ± 0.12 (n=2)		0.166	>25	>50.0	>50.0	This work
2242	Structure above				0.014 +/- 0.0048 (n=2)	0.67 +/- 0.19 (n=2)		1.57	>25	31139	>50.0	This work

*Cytotoxicity data previously published for **1962**, **2062**, **2093**, and **2114** (27)
Reference standard for CRL-8155 cells: Quinacrine EC_{50} = 3.99 ± 2.27 µM (n=14)
Reference standard for HepG2 cells: Quinacrine EC_{50} = 9.76 ± 2.73 µM (n=13)
Reference standard for COX-1: Chloramphenicol EC_{50} = 6.31 ± 0.91 (n=8)
Reference standard for SDH-A: Chloramphenicol EC_{50} = >50 ± 0 (n=8)

920 **Table 5. Physicochemical properties of ring-linker compounds (structures in Table 4)**

Molecule Name	Molecular weight (g/mol)	log P	H-bond donors	H-bond acceptors	Solubility limit @ pH 7.4 (uM)	Solubility limit at pH 2.0 (uM)	Solubility limit @ pH 6.5 (uM)	*Protein binding mouse plasma: % bound	PAMPA: Pe (pH 7.4) (nm/sec)	PAMPA: Pe (pH 5.0) (nm/sec)	Predicted permeability cm/s x 10^4
2114	415.85	3.47	1	4	69.4	78.4	53.8	98.7	319	284	2.394
2067	436.72	4.52	1	3	9.3	10.3	8.8, 9.8	99.7	313	349	3.849
2091	481.18	4.67	1	3		49	<10		226	238	4.500
2093	432.31	3.76	1	4	26.8	60.5, 67.2	39, 51.5	99.9	316	336	2.333
2069	434.3	4.75	1	3	6	39.9, 49.1	36.4, 29.4	99.6	286	288	3.721
2139	456.25	4.34	1	3	26.2	76.8	65	99.5	269	251	3.867
2259	451.83	3.58	1	4	44.4	52	80.6	95.0			2.319
2138	472.7	4.63	1	3	26.2	58.4	33	100.0	235	237	3.887
2258	468.29	3.87	1	4	44.4	> 100	39.2	98.8			2.309
2207	476.36	3.41	2	5		66.3	86.8	98.7			1.322
2240	506.38	3.25	2	6		78.1	83.2	87.7			1.118
2080	434.3	4.65	1	3		> 100	53.6				3.853
2242	509.81	4.68	2	4		43.1	< 10	100.0			1.745
Propranolol	259.35	2.58	2	3					600	200	2.449
Methyclo-thiazide	360.22	0.53	2	5					30	30	0.646

921 *Plasma protein binding for 2069 and 2093 were previously reported (27).

922 **Table 6. Pharmacological properties of ring-linker compounds.** In vitro metabolic
923 stability ($T_{½}$) was measured in mouse and human liver microsomes. Pharmacokinetic
924 studies in mice (n=3 per compound) were done with a single PO dose at 50 mg/kg in
925 MMV vehicle (defined in Methods).

Molecule Name	Mouse microsome stability T1/2 (min)	Human microsome stability T1/2 (min)	Mouse Oral PK: Cmax ± SD (µM)	Mouse Oral PK: AUC ± SD (min*µmol/L)	Mouse Oral PK: Concentrations in pooled mouse feces ± SD (µM)
2114	7.7	15.2	7.5 ± 2.4 (n=3)	1854 ± 103 (n=3)	11.4 ± 4.1 (n=3)
2067	3.1	9.3	65.2 ± 13.3 (n=3)	17263 ± 5167 (n=3)	
2091	2	9.4			
2093	3.2	8.3	5.8 ± 1.54 (n=3)	1863 ± 658 (n=3)	31.1 ± 3.5 (n=3)
2069	3.6	8.2	21.8 ± 8.8 (n=3)	3932 ± 431 (n=3)	
2139	11.7	20.1	40.7 ± 10.6 (n=3)	10404 ± 2589 (n=3)	36.2 ± 3.7 (n=3)
2259	29.4	32.7			25.8 ± 16.2 (n=3)
2138	5.8	15	30.8 ± 1.3 (n=3)	6269 ± 1806 (n=3)	43.6 ± 3.8 (n=3)
2258	13.8	25.5			
2207	5.3	25.1	30.8 ± 6.5 (n=3)	3048 ± 863 (n=3)	
2240	24.2	42.3	11.1 ± 11.8 (n=3)	856 ± 813 (n=3)	846 ± 220 (n=3)
2080	1.6	8	25.4 ± 8.6 (n=3)	5092 ± 1466 (n=3)	17.9 ± 5.4 (n=3)
2242	4.5	7.7	2.5 ± 0.7 (n=3)	512 ± 51 (n=3)	52.7± 16.2 (n=3)

926 *Microsome half-lives for **2093** and **2114** were previously published (27).

927 **Table 7. CYP enzyme inhibition**. The values represent the percent inhibition of the
928 human CYP isoenzymes with compounds **2093**, **2114**, and **2259** at 10 µM
929 concentration.
930

Molecule Name	CYP1A2	CYP2C8	CYP2C9	CYP2D6	CYP3A4
2093	4.1	87.3	13.6	36.0	25.4
2114	4.0	74.7	-9.20	16.6	24.9
2259	10.4	62.1	-13.1	31.6	37.5

931
932
933 **Table 8. hERG inhibition.** The percent inhibition of hERG activity for **2093, 2114**, and
934 **2259** was measure at two concentrations (10 and 30 µM) either without or with bovine
935 serum albumin (BSA).
936

	- BSA		+ BSA	
Molecule Name	10 µM	30 µM	10 µM	30 µM
2093	31.6	62.1	17.9	20.9
2114	28.5	58.8	18.8	23.9
2259	23.1	64.9	12.9	19.5

937

938 **Figure legends**

939

940 **Figure 1. Correlation between *Cp*MetRS inhibition (K_i) and *C. parvum* growth**
941 **inhibition (EC_{50}).**

942

943 **Figure 2. Parasite persistence assay.** Parasite numbers were normalized to
944 numbers of host nuclei over time with increasing concentrations of **2093** (A),
945 nitazoxanide (B), or MMV665917 (C). Below are one-phase exponential decay curves
946 for **2093** (D), nitazoxanide (E) and MMV665917 (F) using parasite persistence assay
947 data normalized to a percentage of the data for the DMSO control at each time point.
948 Compound **2093** has a curve consistent with a potentially parasiticidal mechanism (akin
949 to MMV665917 and dissimilar to nitazoxanide).

950

951 **Figure 3. Efficacy of MetRS inhibitors in murine *C. parvum* (IFN-γ KO) infection**
952 **model.** Adult IFN-γ KO mice (n=3 per group) were infected with luciferase-expressing
953 oocysts on Day 0 and treated orally with vehicle or test compounds at the indicated
954 doses from days 6-10 post-infection. Stools were collected at 24 hour intervals, pooled,
955 and quantitated for luminescent parasites (panels on left). The weights of the mice from
956 the same experiment are shown immediately to the right. Each pair of panels (A-G)
957 represents a separate experiment.
958

959 **Figure 4. Relationship of chemical properties to efficacy for the MetRS inhibitors.**
960 Compounds are color coded as follows: no efficacy in mouse models [< 1 log drop in
961 parasites, red squares (**2067**, **2069**, **2080**, **2169**, **2207**, **2240**, & **2242)**], moderate
962 efficacy [1-2 log drop in parasites, orange triangles (**2138**, **2139**, & **2258**)], and strong
963 efficacy [>2 log drop in parasites, green circles (**2093**, **2114**, & **2259**)]. The predicted
964 permeability is plotted against solubility at pH 6.5/EC_{50}.

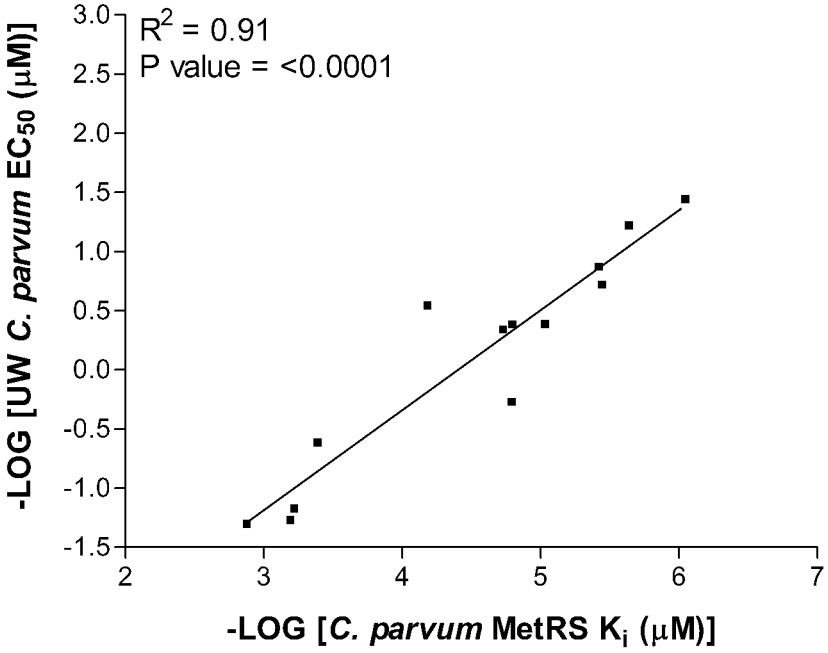

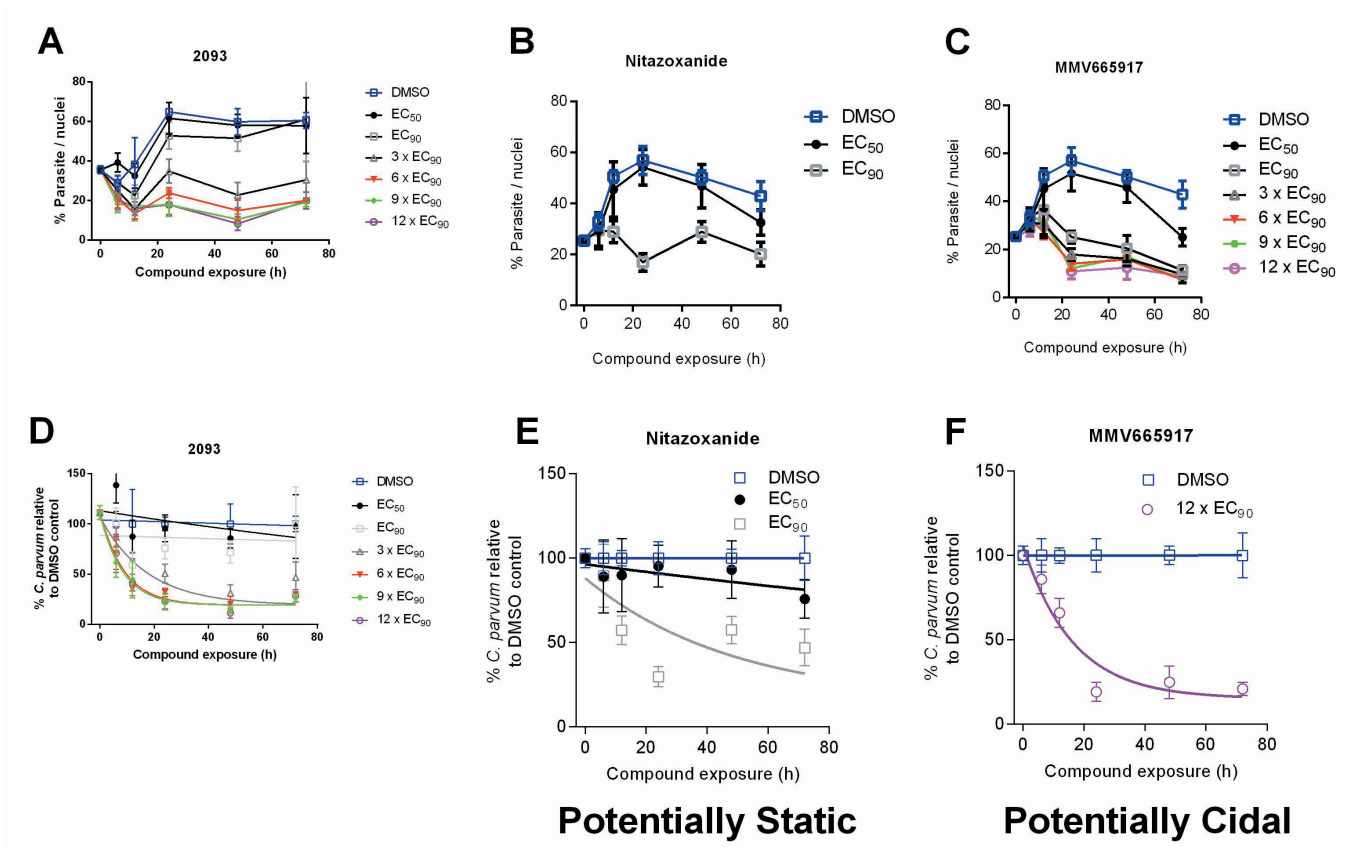

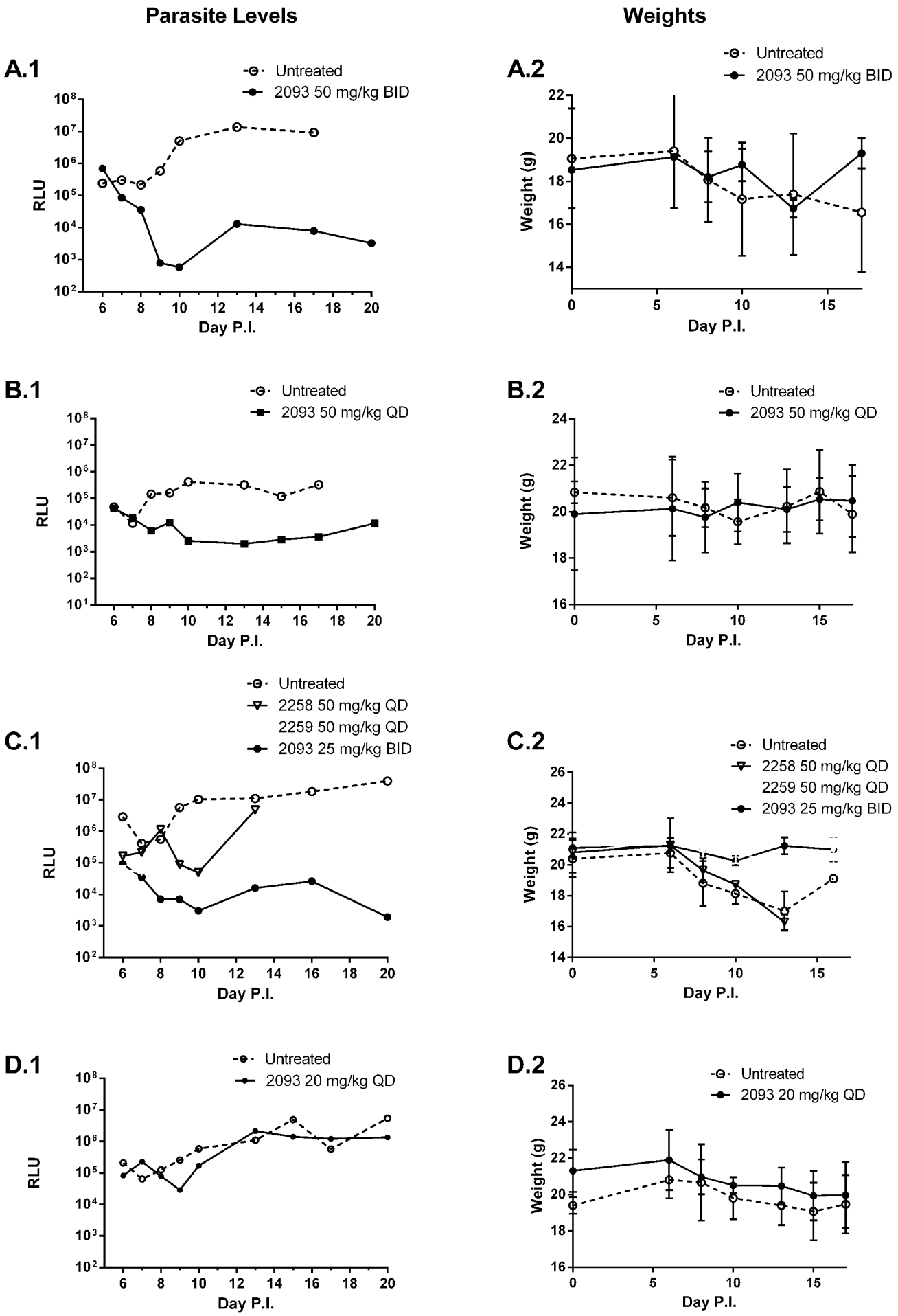

Parasite Levels | **Weights**

E.1

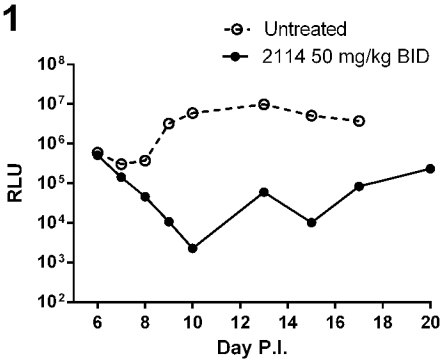

E.2

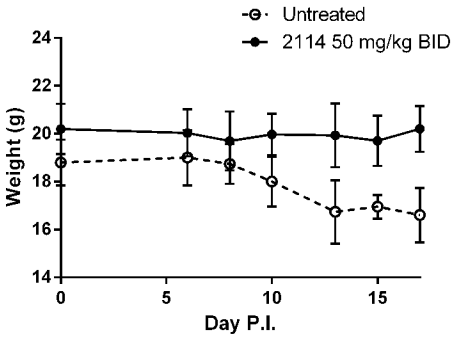

F.1

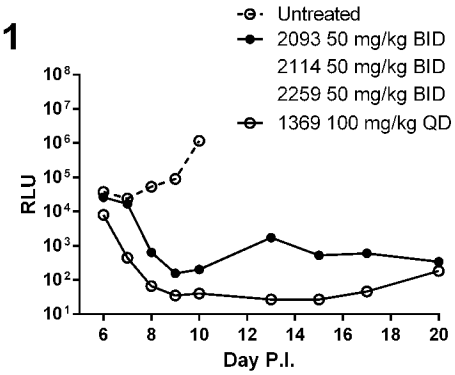

F.2

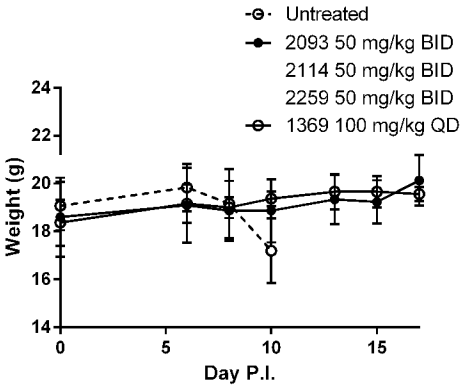

G.1

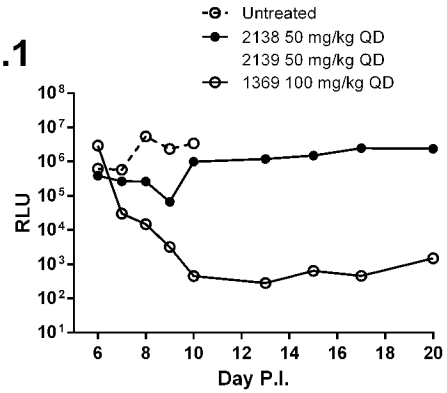

G.2

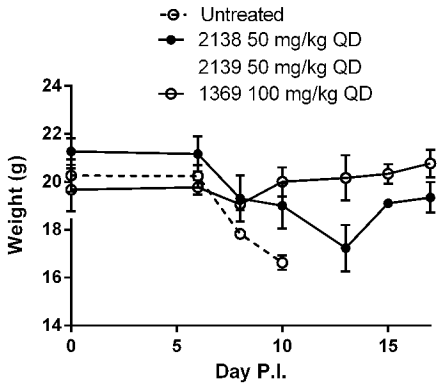

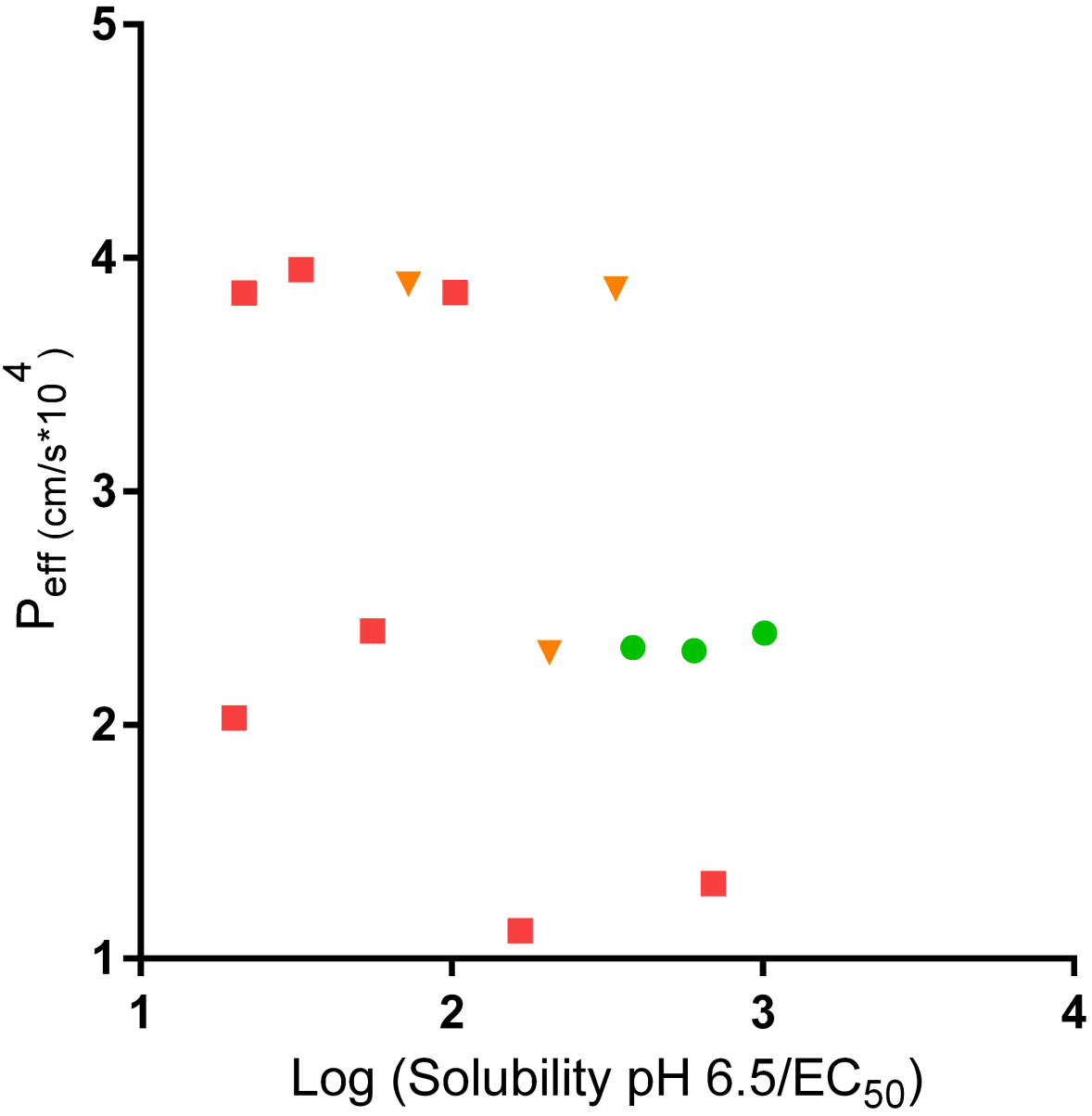

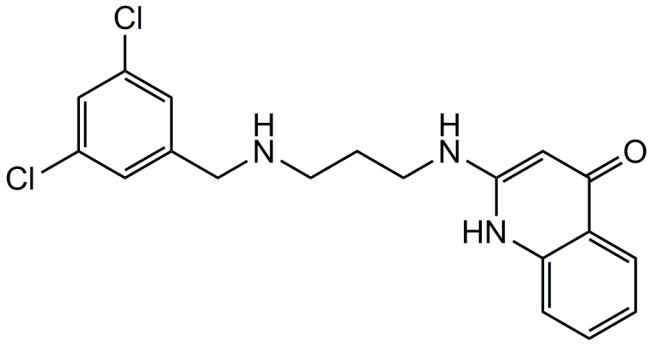

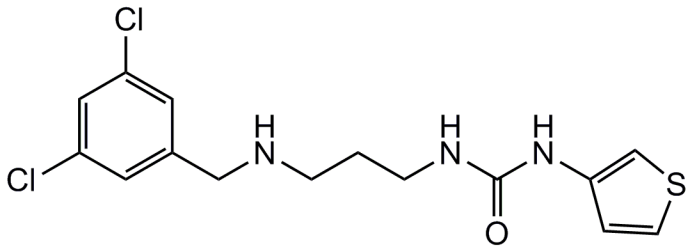

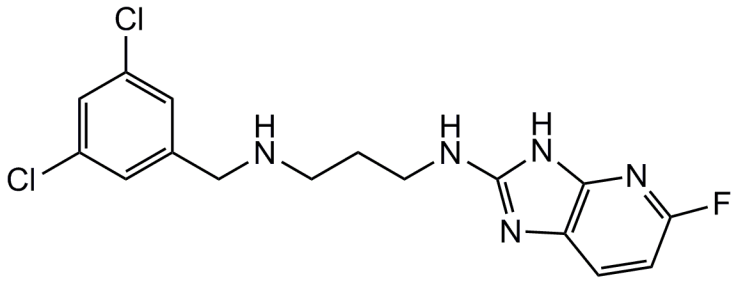

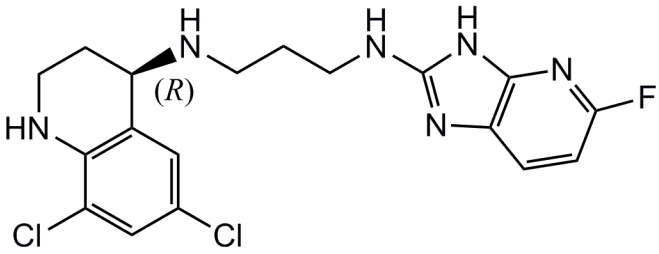

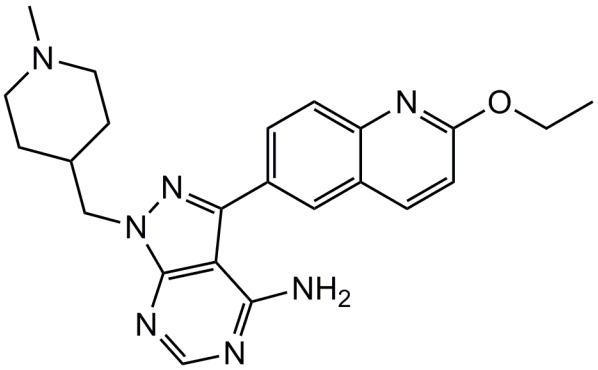

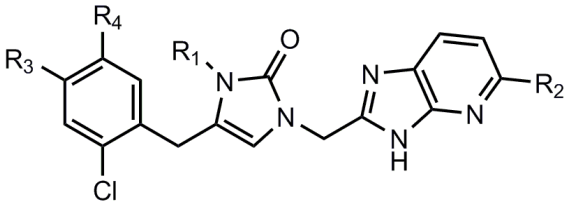

MetRS Inhibitor Scaffold

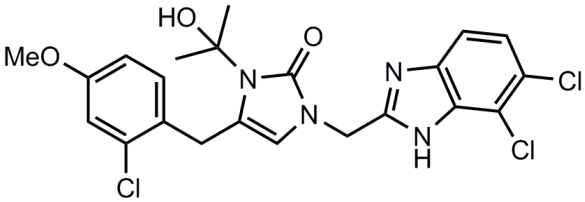

Cmpd 2242